OH-Initiated atmospheric degradation of hydroxyalkyl hydroperoxides: mechanism, kinetics, and structure-activity relationship

Long Chen,[1,2] Yu Huang, *,[1,2] Yonggang Xue, [1,2] Zhihui Jia,[3] Wenliang Wang[4]

[1] *State Key Lab of Loess and Quaternary Geology (SKLLQG), Institute of Earth Environment, Chinese Academy of Sciences (CAS), Xi'an, 710061, China*

[2] *CAS Center for Excellence in Quaternary Science and Global Change, Xi'an, 710061, China*

[3] *School of Materials Science and Engineering, Shaanxi Normal University, Xi'an, Shaanxi, 710119, China*

[4] *School of Chemistry and Chemical Engineering, Key Laboratory for Macromolecular Science of Shaanxi Province, Shaanxi Normal University, Xi'an, Shaanxi, 710119, China*

Submitted to *Atmospheric Chemistry & Physics*

*Corresponding author:

Prof. Yu Huang, E-mail address: huangyu@ieecas.cn

Abstract:

Hydroxyalkyl hydroperoxides (HHPs), formed in the reactions of Criegee intermediates (CIs) with water vapor, play essential roles in the formation of secondary organic aerosol (SOA) under atmospheric conditions. However, the transformation mechanisms for the OH-initiated oxidation of HHPs remain incompletely understood. Herein, the quantum chemical and kinetics modeling methods are applied to explore the mechanisms of the OH-initiated oxidation of the distinct HHPs ($HOCH_2OOH$, $HOCH(CH_3)OOH$ and $HOC(CH_3)_2OOH$) formed from the reactions of CH_2OO, *anti*-CH_3CHOO and $(CH_3)_2COO$) with water vapor. The calculations show that the dominant pathway is H-abstraction from the -OOH group in the initiation reactions of OH radical with $HOCH_2OOH$ and $HOC(CH_3)_2OOH$. H-abstraction from the -CH group is competitive with that from the -OOH group in the reaction of OH radical with $HOCH(CH_3)OOH$. The barrier of H-abstraction from the -OOH group slightly increases when the number of methyl groups increase. In pristine environments, the self-reaction of RO_2 radical initially produces a tetroxide intermediate via an oxygen-to-oxygen coupling, then it decomposes into propagation and termination products through asymmetric two-step O-O bond scission, in which the rate-limiting step is the first O-O bond cleavage. The barrier height of the reactions of distinct RO_2 radicals with HO_2 radical is not affected by the number of methyl substitutions. In urban environments, the reaction with O_2 to form formic acid and HO_2 radical is the dominant removal pathway for $HOCH_2O$ radical formed from the reaction of $HOCH_2OO$ radical with NO. The β-site C-C bond scission is the dominant pathway in the dissociation of the $HOCH(CH_3)O$ and $HOC(CH_3)_2O$ radicals formed from the reactions of NO with $HOCH(CH_3)OO$ and $HOC(CH_3)_2OO$ radicals. These new findings deepen our understanding of the photochemical oxidation of hydroperoxides under realistic atmospheric conditions.

1. Introduction

Hydroxyalkyl hydroperoxides (HHPs), formed in the reactions of Criegee intermediates (CIs) with water vapor and in the initiation OH-addition with subsequent HO_2-termination reactions, play important roles in the formation of secondary organic aerosol (SOA) (Qiu et al., 2019; Kumar et al., 2014). The CIs formed from the ozonolysis of alkenes are characterized by high reactivity and excess energy, which can either prompt the unimolecular decay to OH radical or, after collisional stabilization, bimolecular reactions with various trace gases such as SO_2, NO_2, and H_2O to produce sulfate, nitrate and SOA, thereby influencing air quality and human health (Lester and Klippenstein, 2018; Chen et al., 2017, 2019; Liu et al., 2019; Chhantyal-Pun et al., 2017; Anglada and Solé, 2016; Gong and Chen, 2021). Among these reactions, the bimolecular reaction of CIs with water is regarded as the dominant chemical sink, since its concentration (1.3-8.3 $\times 10^{17}$ molecules cm^{-3}) is several orders of magnitude greater than those of SO_2 and NO_2 (~ 10^{12} molecules cm^{-3}) in the atmosphere (Huang et al., 2015; Khan et al., 2018; Taatjes et al., 2013, 2017). The primary products of the reaction of CIs with water are highly oxygenated HHPs, which are difficult to detect and identify through the available analytical techniques because of their thermal instability (Qiu et al., 2019; Anglada and Solé, 2016; Chao et al., 2015; Chen et al., 2016a; Ryzhkov and Ariya, 2003).

Due to the presence of both hydroxyl and perhydroxy moieties, HHPs have relatively low volatility and contribute significantly to the formation of SOA (Qiu et al., 2019). The atmospheric degradation of HHPs initiated by OH radical is expected to be one of the dominant loss processes because OH radical is the powerful oxidizing agent (Gligorovski et al., 2015; Allen et al., 2018). The reaction with OH radical includes three possible H-abstraction channels, namely the (a) alkyl hydrogen, (b) -OH hydrogen, and (c) -OOH hydrogen, which are followed by further reactions to generate organic peroxy radicals (RO_2) as reactive intermediates (Allen et al., 2018). On the basis of our current mechanistic understanding, RO_2 radicals have three possible channels in pristine environments: (1) RO_2 radicals can proceed self- and

cross-reactions to generate alkoxy radical RO, alcohol, carbonyl, and accretion products (Berndt et al., 2018; Zhang et al., 2012; Valiev et al., 2019); (2) RO_2 radicals can react with HO_2 radical to form closed-shell hydroperoxide (ROOH), RO radical, OH radical, etc.; (Dillon and Crowley, 2008; Iyer et al., 2018) (3) RO_2 radicals can undergo autoxidation through intramolecular H-shift and alternating O_2-addition steps to produce highly oxygenated organic molecules (HOMs), which have been identified as the low volatility compounds that contribute to the formation of SOA (Crounse et al., 2013; Jokinen et al., 2014; Wang et al., 2018; Ehn et al., 2014; Iyer et al., 2021). In urban environments, RO_2 radicals can react with NO_x to generate peroxynitrate (RO_2NO_2), organic nitrate ($RONO_2$), RO radicals and other SOA precursors (Wang et al., 2017; Xu et al., 2014, 2020; Ma et al., 2021). The relative importance of distinct pathways is highly dependence on the nature of RO_2 radicals and the concentrations of coreactants.

Hydroxymethyl hydroperoxide (HMHP, $HOCH_2OOH$), the simplest HHP derived from the ozonolysis of all terminal alkenes in the presence of water, is observed in significant abundance in the atmosphere (Allen et al., 2018). The measured concentration of HMHP is varied considerably depending on the location, season and altitude, and its concentration has been reported to be as high as 5 ppbv in forested regions (Allen et al., 2018; Francisco and Eisfeld, 2009). In one study, the concentration of HMHP was measured during the summer of 2013 in the Southeastern United States, and it was found that the average mixing ratio of HMHP was 0.25 ppbv with a maximum of 4.0 ppbv in the boundary layer (Allen et al., 2018). Allen et al. (2018) conducted the OH-initiated oxidation of HMHP in an environmental chamber and simulated the effect of HMHP oxidation on global formic acid production by applying the chemical transport model GEOS-Chem. They found that H-abstraction from the methyl group of HMHP results in the formation of formic acid and contributes approximately 1.7 Tg yr^{-1} to global formic acid production. Francisco and Eisfeld (2009) employed the *ab initio* CCSD(T)//MP2 methods to study the atmospheric oxidation mechanism of HMHP initiated by OH radical, and they also concluded that the degradation of HMHP can contribute to the formation of formic

acid in the atmosphere. Additionally, the unimolecular decomposition of HMHP is another key removal process in the atmosphere. Chen et al. (2016b) found that the formation of CH_2O and H_2O_2 is more preferable than the production of HCOOH and H_2O. Kumar et al. (2014) also concluded that the aldehyde- or ketone-forming pathway is kinetically favored over the carboxylic acid-forming channel in the unimolecular decomposition of various HHPs. All of the above milestone investigations offer highly useful information on the decomposition of HHPs in the gas phase. However, to the best of our knowledge, there are few studies on the subsequent transformations of the resulting H-abstraction products formed from the OH-initiated oxidation of larger HHPs. The effect of the size and number of substituents on the rates and outcomes of SOA precursors (e.g. ROOR, HOMs) is uncertain up to now. Therefore, it is necessary to evaluate the potential of larger HHPs and their oxidation products to substantial SOA formation under different NO_x conditions.

In the present study, the mechanisms and kinetics of distinct HHPs oxidation initiated by OH radical are investigated by employing quantum chemical and kinetics modeling methods. For the resulting H-abstraction products RO_2 radicals, the subsequent reactions involving self-reaction, isomerization and reaction with HO_2 radical are considered in the absence of NO, while the subsequent reactions including addition, decomposition and H-abstraction by O_2 are considered in the presence of NO. The HHPs investigated in the present study are generated from the bimolecular reactions of distinct carbonyl oxides (CH_2OO, *anti*-CH_3CHOO and $(CH_3)_2COO$) with water vapor.

2. Computational details

2.1 Electronic structure and energy calculations

The equilibrium geometries of all the open-shell species, including reactant (R), pre-reactive complex (RC), transition state (TS), post-reactive complex (PC), and product (P), are fully optimized at the unrestricted M06-2X/6-311+G(2df,2p) level of theory (UM06-2X) (Zhao and Truhlar, 2006; Zheng and Truhlar, 2009), whereas all

the closed-shell species are optimized at the restricted M06-2X/6-311+G(2df,2p) level of theory (RM06-2X). This is because the M06-2X functional has been proven to be reliable for describing thermochemistry, kinetics and non-covalent interactions (Zhao and Truhlar, 2008). Harmonic vibrational frequencies are performed at the same level to verify that each stationary point is either a true minima (with no imaginary frequency) or a transition state (with one imaginary frequency). Zero-point vibrational energy (ZPVE) and Gibbs free energy corrections (G_{corr}) from harmonic vibrational frequencies are scaled by a factor of 0.98 (Zhao and Truhlar, 2006). Intrinsic reaction coordinate (IRC) calculations are performed to verify the connection between the transition state and the designated reactant and product (Fukui, 1981). The single-point energies are calculated at the (U/R)M06-2X/ma-TZVP level of theory (Zheng, et al., 2011).

The tetroxide intermediate formed from the self-reaction of RO_2 radical proceeds through asymmetric two step O-O bond scission to produce a caged tetroxide intermediate of overall singlet multiplicity comprising two same-spin alkoxyl radicals (spin down) and triplet oxygen (spin up). This type of reaction mechanism can be described by broken symmetry unrestricted DFT (UDFT) and multi-reference CASSCF methods (Lee, et al., 2016; Bach, et al., 2005). Previous studies have demonstrated that the UDFT method is suitable for identifying the minimum of a metastable singlet caged radical complex and the transition state of O-O bond homolysis, and the resulting energies obtained using the UDFT method are comparable to those obtained using the more accurate and expensive CASSCF method (Lee, et al., 2016; Bach, et al., 2005). In the present study, the UDFT method, which provides a balance between computational accuracy and efficiency, is selected to study asymmetric O-O bond scission. The broken symmetry UM06-2X/6-311+G(2df,2p) method is applied to generate the initial guesses for the geometries of the tetroxide intermediate and transition state with mixed HOMO and LUMO ($S^2 \approx 1$) by using the guess = mix keyword. The single-point energies are refined at the UM06-2X/ma-TZVP level of theory.

To further evaluate the reliability of the employed method for predicting the

reaction mechanisms, the single-point energies of all the stationary points involved in the initiation reactions of OH radical with distinct HHPs are recalculated at the (U/R)CCSD(T)/6-311+G(2df,2p) level of theory based on the (U/R)M06-2X optimized geometries. Furthermore, the stability of the pre-reactive complexes is assessed by performing basis set superposition error (BSSE) using counterpoise method (Boys and Bernardi, 1970). For simplicity, no prefix is used throughout this article. Herein, the Gibbs free energy (G) for each species is obtained by combining the single-point energy with the Gibbs correction ($G = G_{corr} + E$). The electronic energy ($\Delta E_a^{\#}$) and free energy ($\Delta G_a^{\#}$) barriers are defined as the difference in energy between transition state and pre-reactive complex ($\Delta E_a^{\#} = E_{TS} - E_{RC}$ and $\Delta G_a^{\#} = G_{TS} - G_{RC}$). The reaction free energy (ΔG) is referred to the difference in energy between product and reactant ($\Delta G = G_P - G_R$). The calculated $\Delta E_a^{\#}$ and $\Delta G_a^{\#}$ for the initiation H-abstraction pathways are summarized in Table S1. As shown in Table S1, the mean absolute deviations (MADs) of $\Delta E_a^{\#}$ and $\Delta G_a^{\#}$ between the CCSD(T)/6-311+G(2df,2p) and M06-2X/ma-TZVP approaches are 0.43 and 0.45 kcal·mol^{-1}, respectively; the largest deviations of $\Delta E_a^{\#}$ and $\Delta G_a^{\#}$ are 1.2 and 1.1 kcal·mol^{-1}, respectively. These results reveal that the energies obtained using the M06-2X/ma-TZVP method are in good accord with those obtained using the gold-standard coupled-cluster approach CCSD(T) within the uncertainties of systematic errors. Therefore, the M06-2X/ma-TZVP method is selected to investigate the atmospheric degradation of HHP initiated by OH radical under different conditions. In the following sections, $\Delta G_a^{\#}$ is applied to construct the reaction profiles unless otherwise stated.

For the H-shift reactions of RO_2 radicals, reactants, transition states and products have multiple conformers. Previous literature has demonstrated that the reaction kinetics of multiconformers involvement are more precise than that of single conformer approximation (Møller, et al., 2016, 2020). Herein, the multiconformer treatment is performed to investigate the H-shift reactions of RO_2 radicals. A conformer search within the Molclus program is employed to generate a pool of conformers for RO_2 radicals (Lu, 2020). The selected conformers are further optimized at the M06-2X/6-311+G(2df,2p) level of theory, followed by single-point

energy calculations at the M06-2X/ma-TZVP level of theory. On the basis of the calculated Gibbs free energies, the Boltzmann populations (w_i) of each RO_2 conformer is expressed as eqn 1.

$$w_i = \frac{e^{-\Delta G_i / k_B T}}{\sum_i e^{-\Delta G_i / k_B T}} \quad (1)$$

where ΔG_i is the relative Gibbs free energy of conformer i, k_B is the Boltzmann's constant, and T is temperature in Kelvin. All the quantum chemical calculations are performed by using the Gaussian 09 program (Frisch, et al., 2009).

2.2 Kinetics calculations

The rate coefficients of unimolecular reactions are calculated by using the Rice-Ramsperger-Kassel-Marcus theory coupled with energy-grained master equation (RRKM-ME) method (Holbrook, 1996), and the rate coefficients of bimolecular reactions are determined by utilizing the traditional transition state theory (TST) (Fernández-Ramos, 2007). RRKM-ME calculations are performed by using the MESMER 6.0 program (Glowacki, et al., 2012). N_2 is used as the buffer gas. A single exponential down model is employed to simulate the collision energy transfer ($<\Delta E>_{down}$ = 200 cm^{-1}). The collisional Lennard-Jones parameters are estimated by using an empirical formula proposed by Gilbert and Smith (1990). For the H-shift reactions of RO_2 radicals, the rate coefficients are determined by employing the multiconformer transition state theory (MC-TST) approach (Møller, et al., 2016). The MC-TST rate coefficient $k_{MC\text{-}TST}$ is calculated by the sum of individual intrinsic reaction coordinate TST (IRC-TST) rate coefficient $k_{IRC\text{-}TST}$, each weighted by the Boltzmann population of the corresponding RO_2 conformer (Møller, et al., 2016).

$$k_{MC\text{-}TST} = \sum_{i}^{\text{all TS conf.}} w_i \times k_{IRC\text{-}TST i} \quad (2)$$

where $k_{IRC\text{-}TST i}$ represents the rate coefficient of conformer i, and w_i is the relative Boltzmann population of the corresponding reactant connected to TS_i. The one-dimensional asymmetry Eckart model is employed to calculate the tunneling correction (Eckart, 1930). Considering the uncertainty in barrier heights (~ 1.0

kcal mol^{-1} by the M06-2X method) and in tunneling corrections, the uncertainty of the calculated rate coefficient is about one order of magnitude in the present study.

3. Results and discussion

3.1 Initiation reaction of HHPs with OH radical

Previous literatures have proposed that the lifetime of CI with respect to the reaction with water vapor exhibits strong dependence on the nature of CI (Anglada and Solé, 2016; Taatjes, et al., 2013; Anglada, et al., 2011), and the primary product is HHPs in both the gas phase and air-water interfaces (Chao, et al., 2015; Chen, et al., 2016a; Smith et al., 2015; Zhu et al., 2016; Zhong et al., 2018). In the present study, we mainly consider three kinds of HHPs originated from the addition of water to CH_2OO and methyl-substituted CI (*anti*-CH_3CHOO and $(CH_3)_2COO$). The lowest-energy conformers HHP ($HOCH_2OOH$, $HOCH(CH_3)OOH$ and $HOC(CH_3)_2OOH$) are obtained from the previous study as shown in Figure 1 (Chen et al., 2019), and they are selected as the model system to investigate the atmospheric degradation mechanism of HHP initiated by OH radical. Letters and numbers are used to label carbon, oxygen and hydrogen atoms at different reaction sites.

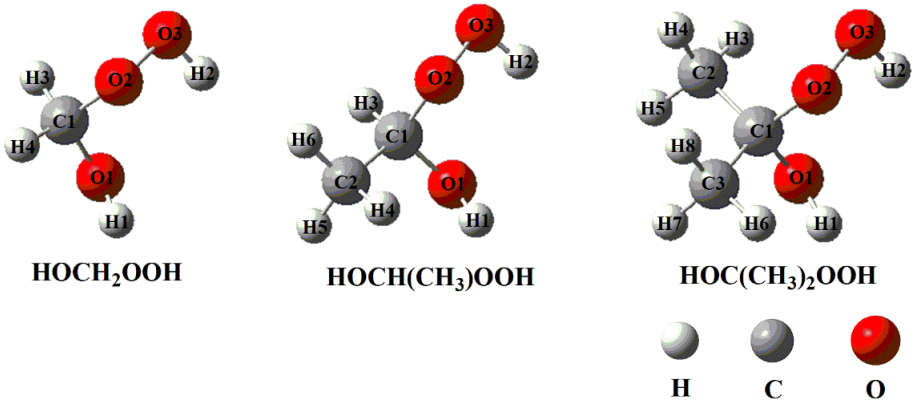

Figure 1. The structures of distinct HHPs

The free-energy and electronic-energy potential energy surfaces (PESs) for the initiation reactions of OH radical with $HOCH_2OOH$, $HOCH(CH_3)OOH$ and $HOC(CH_3)_2OOH$ are presented in Figures 2-4 and S1-S3, respectively. The optimized geometries of all the stationary points are displayed in Figures S6-S8, respectively. As can be seen in Figure 2, the reaction of $HOCH_2OOH$ with OH radical proceeds

through four pathways: H-abstraction from the -O_1H_1 (R1), -C_1H_3 (R2), -C_1H_4 (R3) and -$O_2O_3H_2$ (R4) groups. For each pathway, a pre-reactive complex with a six- or seven-membered ring structure is formed in the entrance channel, which is stabilized by hydrogen bond interactions between the oxygen atom of OH radical and the abstraction hydrogen atom of $HOCH_2OOH$, and between the remnant hydrogen atom of OH radical and one of the oxygen atoms of $HOCH_2OOH$ (Figure S6). Then, it surmounts the modest barrier that is higher in energy than the reactants to reaction. The reaction barriers $\Delta G_a^{\#}$ decrease in the order of 6.4 (R1) > 5.8 (R2) ≈ 5.4 (R3) > 1.5 (R4) kcal·mol^{-1}, indicating that H-abstraction from the -$O_2O_3H_2$ group (R4) is more preferable than those from the -O_1H_1, -C_1H_3 and -C_1H_4 groups (R1-R3). The same conclusion is also derived from the energy barriers $\Delta E_a^{\#}$ that R4 is the most favorable H-abstraction pathway (Figure S1). The difference in barrier heights can be attributed to the bond dissociation energy (BDE) of the multiple types of bonds in $HOCH_2OOH$ molecule. BDE decreases in the order of 103.7 (O_1-H_1) > 98.2 (C_1-H_3) ≈ 97.4 (C_1-H_4) > 87.2 (O_3-H_2) kcal·mol^{-1}, and this order is consistent with that of the barrier heights of H-abstraction reactions. Their reaction free energy values indicate that the exothermicity of R4 is the largest among these four H-abstraction reactions. Based on the above discussions, it is concluded that H-abstraction from the -$O_2O_3H_2$ group resulting in the formation of $HOCH_2OO$ radical (R4) is feasible both thermodynamically and kinetically.

Given the multiple reaction sites of hydrogen atoms, the atmospheric transformation of $HOCH(CH_3)OOH$ from the *anti*-CH_3CHOO + H_2O reaction should have six possible H-abstraction pathways as presented in Figure 3. As shown in Figure 3, each H-abstraction reaction begins with the formation of a weakly bound hydrogen bonded pre-reactive complex with a six- or seven-membered ring structure in the entrance channel (Figure S7). Then it immediately transforms into the respective product via the corresponding transition state. The $\Delta G_a^{\#}$ of H-abstraction from the -C_1H_3 (R6) and -$O_2O_3H_2$ (R8) groups are 2.2 and 1.7 kcal·mol^{-1}, respectively, which are ~ 4-5 kcal·mol^{-1} lower than those from the -O_1H_1 (R5) and -CH_3 (R7) groups. This result shows that R6 and R8 have nearly identical importance in the

atmosphere. Compared with the barriers of H-abstraction at the C_α (R6) and C_β (R7) positions, it can be found that the former case is more favourable than the latter case. This conclusion is further supported by Jara-Toro's study for the reactions of OH radical with linear saturated alcohols (methanol, ethanol and n-propanol) that H-abstraction at the C_α position is predominant (Jara-Toro, et al., 2017, 2018).

For the OH-initiated oxidation of $HOCH(CH_3)OOH$ from the *syn*-CH_3CHOO + H_2O reaction, the corresponding free-energy and electronic-energy PESs are displayed in Figures S4 and S5, respectively. From Figure S4, it can be seen that H-abstraction by OH radical from $HOCH(CH_3)OOH$ has six possible pathways. For each pathway, a per-reactive complex is formed prior to the corresponding transition state, and then it overcomes a modest barrier to reaction. The $\Delta G_a^{\#}$ of R6' and R8' are 2.3 and 1.8 kcal mol^{-1}, respectively, which are about 5 kcal mol^{-1} lower than those of R5' and R7'. The result shows that H-abstraction from the -CH (R6') and -OOH (R8') groups is preferable kinetically. The same conclusion is also derived from the energy barriers $\Delta E_a^{\#}$ that the R6' and R8' are the most favourable H-abstraction pathways (Figure S5). It should be noted that although the barriers of R6' and R8' are comparable, the exoergicity of R6' is significantly lower than that of R8'. The aforementioned conclusions are consistent with the results derived from the OH-initiated oxidation of $HOCH(CH_3)OOH$ from the *anti*-CH_3CHOO + H_2O reaction. Zhou et al. (2019) demonstrated that the bimolecular reaction of *syn*-CH_3CHOO with water leading to the formation of $HOCH(CH_3)OOH$ is of less importance in the atmosphere, while the unimolecular decay to OH radical is the major loss process of *syn*-CH_3CHOO. Therefore, in the present study, we mainly focus on the subsequent mechanism of intermediates generated from OH-initiated oxidation of $HOCH(CH_3)OOH$ from the *anti*-CH_3CHOO + H_2O reaction.

From Figure 4, it can be seen that H-abstraction from $HOC(CH_3)_2OOH$ has eight possible H-abstraction pathways. All the H-abstraction reactions are strongly exothermic and spontaneous, suggesting that they are thermodynamically feasible under atmospheric conditions. It deserves mentioning that the release of energy of R12 is significantly greater than that of R9-R11. For each H-abstraction pathway, an

RC with a six- or seven-membered ring structure is formed prior to the corresponding TS, which is more stable than the separate reactants due to the hydrogen bond interactions between $HOC(CH_3)_2OOH$ and OH radical. Then, the RC overcomes a modest barrier to reaction. The $\Delta G_a^{\#}$ of H-abstraction from the $-O_2O_3H_2$ group (R12) is 2.7 kcal mol^{-1}, which is the lowest among these eight H-abstraction reactions. This result again shows that H-abstraction from the $-O_2O_3H_2$ group is the dominant pathway.

The rate coefficients of each H-abstraction pathway involved in the initiation reactions of distinct HHPs with OH radical are estimated over the temperature range from 273 to 400 K as summarized in Table S2-S4 and Figures S9-S11. As shown in Table S2, the total rate coefficients k_{tot} of $HOCH_2OOH$ reaction with OH radical decrease slightly with increasing temperature. At ambient temperature, k_{tot} is estimated to be 3.3×10^{-11} cm^3 molecule^{-1} s^{-1}, which is greater by a factor of ~5 than that reported by Allen et al. (2018) ($(7.1 \pm 1.5) \times 10^{-12}$ cm^3 molecule^{-1} s^{-1}, at 295 K), who derived the result from the reaction of HMHP with OH radical through CF_3O^- chemical ionization mass spectrometry (CIMS) and laser-induced fluorescence (LIF). This discrepancy can be attributed to the uncertainties associated with the barrier height and tunneling correction. $k_{R4(O3\text{-}H2)}$ is one to two orders of magnitude greater than $k_{R1(O1\text{-}H1)}$, $k_{R2(C1\text{-}H3)}$ and $k_{R3(C1\text{-}H4)}$ in the whole temperature range, indicating that R4 is the most favorable H-abstraction pathway. For example, $k_{R4(O3\text{-}H2)}$ is calculated to be 2.9×10^{-11} cm^3 molecule^{-1} s^{-1} at 298 K, which is higher than $k_{R1(O1\text{-}H1)}$ (1.8×10^{-13}), $k_{R2(C1\text{-}H3)}$ (9.9×10^{-13}) and $k_{R3(C1\text{-}H4)}$ (2.0×10^{-12}) by 161, 29 and 15 times, respectively.

From Table S3, it can be seen that the total rate coefficients k'_{tot} of $HOCH(CH_3)OOH$ reaction with OH radical decrease in the range between 4.5×10^{-11} (273 K) and 8.1×10^{-12} (400 K) cm^3 molecule^{-1} s^{-1} with increasing temperature, and they exhibit a slightly negative temperature dependence. $k_{R8(O3\text{-}H2)}$ are approximately identical to k'_{tot} in the full temperature range, and they are greater than $k_{R5(O1\text{-}H1)}$, $k_{R6(C1\text{-}H3)}$, $k_{R7\text{-}1(C2\text{-}H4)}$, $k_{R7\text{-}2(C2\text{-}H5)}$ and $k_{R7\text{-}3(C2\text{-}H6)}$ by one to two orders of magnitude. The result also demonstrates that H-abstraction from the -OOH group (R8) is preferable

kinetically. It should be noted that although the barriers of R8 and R6 are comparable, $k_{R8(O3\text{-}H2)}$ is greater than $k_{R6(C1\text{-}H3)}$ by approximately one order of magnitude over the temperature range studied. The most likely reason is the stability of pre-reactive complexes that IM8-a is more stable than IM6-a in energy. A similar conclusion is derived from the rate coefficients of the $HOC(CH_3)_2OOH$ + OH reaction that H-abstraction from the -OOH group (R12) is favorable kinetically (Table S4). The atmospheric lifetimes of $HOCH_2OOH$, $HOCH(CH_3)OOH$ and $HOC(CH_3)_2OOH$ reactivity toward OH radical are estimated to be 0.58-1.74 h, 0.60-1.79 h and 1.23-3.69 h, respectively, at room temperature under typical OH radical concentrations of 5-15 $\times 10^6$ molecules cm^{-3} during daylight (Long et al., 2017).

In summary, the dominant pathway is H-abstraction from the -OOH group in the initiation reactions of OH radical with $HOCH_2OOH$. H-abstraction from the -CH group is competitive with that from the -OOH group in the reaction of OH radical with $HOCH(CH_3)OOH$. Compared with the barriers of H-abstraction from the -OOH and $-CH_2$ groups in the reaction of OH radical with $HOCH_2OOH$, the barrier of H-abstraction from the -CH group is reduced by 3.6 kcal mol^{-1}, whereas the barrier of H-abstraction from the -OOH group is increased by 0.2 kcal mol^{-1} when a methyl group substitution occurs at the C_1-position of $HOCH_2OOH$. The dominant pathway is H-abstraction from the -OOH group in the reaction of OH radical with $HOC(CH_3)_2OOH$, and its barrier height is increased by 1.2 kcal mol^{-1} compared with the OH + $HOCH_2OOH$ system. The barrier of H-abstraction from the -OOH group slightly increases when the number of methyl groups increases. It is interesting to compare the rate coefficient of the dominant pathway in the OH + $HOCH_2OOH$ system with those of the analogous reactions in the OH + $HOCH(CH_3)OOH$ and OH + $HOC(CH_3)_2OOH$ reactions. It can be found that the rate coefficient is almost identical when a methyl group substitution occurs at the C_1-position, whereas the rate coefficient decreases by a factor of 2-5 when two methyl groups are introduced at the C_1-position.

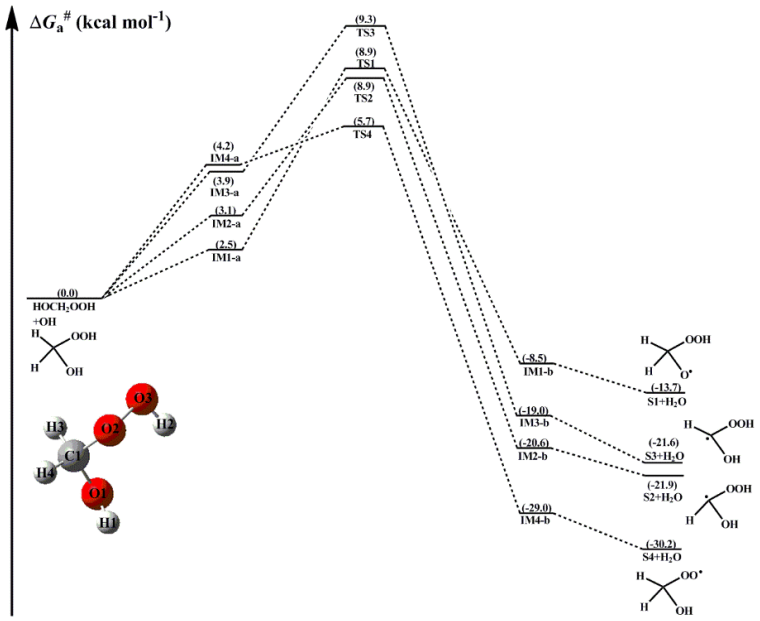

Figure 2. PES ($\Delta G_a^{\#}$) for the OH-initiated reactions of $HOCH_2OOH$ from the CH_2OO + H_2O reaction predicted at the M06-2X/ma-TZVP//M06-2X/6-311+G(2df,2p) level of theory (a and b represent the pre-reactive and post-reactive complexes)

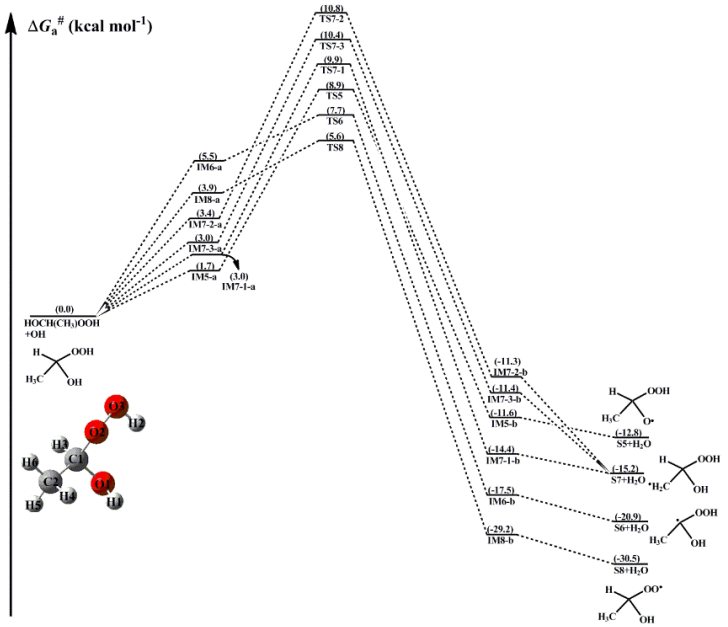

Figure 3. PES ($\Delta G_a^{\#}$) for the OH-initiated reactions of $HOCH(CH_3)OOH$ from the *anti*-CH_3CHOO + H_2O reaction predicted at the M06-2X/ma-TZVP//M06-2X/6-311+G(2df,2p) level of theory (a and b represent the pre-reactive and post-reactive complexes)

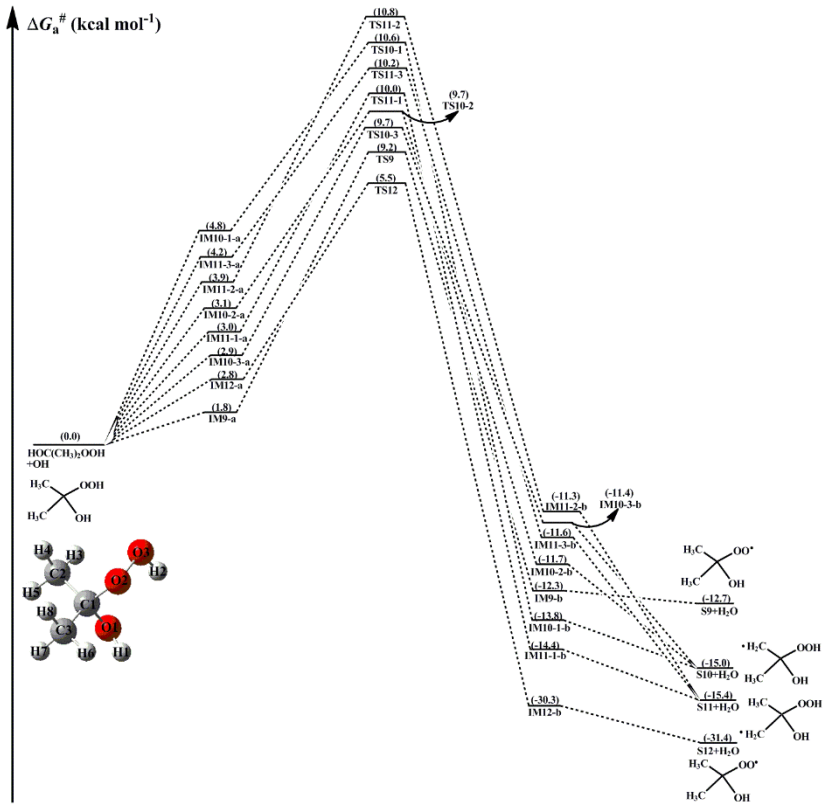

Figure 4. PES ($\Delta G_a^{\#}$) for the OH-initiated reactions of $HOC(CH_3)_2OOH$ from the $(CH_3)_2COO$ + H_2O reaction predicted at the M06-2X/ma-TZVP//M06-2X/6-311+G(2df,2p) level of theory (a and b represent the pre-reactive and post-reactive complexes)

3.2 Subsequent reactions of H-abstraction products RO_2 radicals in pristine environments

In principle, the H-abstraction products RO_2 radicals have three possible fates in pristine environments: (1) the self-reactions of RO_2 radicals can either produce RO + R'O + O_2 (propagation channel), or generate ROH + R'(-H, =O) + O_2 or produce ROOR + O_2 (termination channel) that is recognized as an important SOA precursor (Berndt et al., 2018; Zhang et al., 2012); (2) the RO_2 radicals react with HO_2 radical to form hydroperoxide ROOH, alcoW hol, OH and other products (iniberg et al., 2016; Chen et al., 2021); (3) the RO_2 radicals undergo autoxidation through intramolecular H-shift and alternating O_2 addition steps to generate HOMs (Ehn et al., 2014; Bianchi et al., 2019; Nozière and Vereecken, 2019; Rissanen et al., 2014). The three aforementioned reactions are discussed in further detail in the subsequent subsections.

3.2.1 Reactions mechanism for the self-reaction of RO_2 radicals

The self-reaction is a dominant removal pathway for RO_2 radicals under low concentrations of NO and high concentrations of RO_2 radicals. The self-reaction of RO_2 radicals usually follows the Russell mechanism (Russell, 1957), and has four main possible pathways: (1) $2RO_2 \rightarrow 2RO + O_2$; (2) $2RO_2 \rightarrow ROH + R'CO + O_2$; (3) $2RO_2 \rightarrow ROOR + O_2$; and (4) $2RO_2 \rightarrow ROOH + R'CHOO$ (Atkinson and Arey, 2003). The relative importance of different pathways varies considerably depending on the nature of RO_2 radicals (Valiev et al., 2019; Lee et al., 2016). A schematic PES for the self-reaction of $HOCH_2OO$ radical is drawn in Figure 5. As can be seen in Figure 5a, the self-reaction of $HOCH_2OO$ radical starts with the formation of tetroxide complexes IM13-a and IM14-a in the entrance channel, with 2.9 and 3.4 kcal mol^{-1} stability. Then they fragment into dimer S13 + $^1O_2$ (R13) and $HOCH_2OOH$ + HOCHOO (R14) via TS13 and TS14 with the barriers of 43.3 and 51.5 kcal mol^{-1}, respectively. However, the barriers of R13 and R14 are extremely high, making them irrelevant in the atmosphere.

From Figure 5b, it is seen that the self-reaction of $HOCH_2OO$ radical proceeds via oxygen-to-oxygen coupling leading to the formation of tetroxide intermediate S14 with the electronic-energy and free-energy barriers of 7.3 and 19.6 kcal mol^{-1}. Kumar and Francisco reported an electronic-energy barrier of 14.0 kcal mol^{-1} for the gas phase decomposition of $HOCH_2OO$ radical, which may be a new source of HO_2 radical in the troposphere (Kumar and Francisco, 2015, 2016). Compared with the electronic-energy barriers of the unimolecular dissociation of $HOCH_2OO$ radical and its self-reaction, it can be found that the self-reaction of $HOCH_2OO$ radical resulting in the formation of S14 is significantly feasible. The formed S14 can fragment into $HOCH_2O$ + HCOOH + HO_2 via a concerted process of O_2-O_3 and O_5-O_6 bonds rupture and O_3-H_6 bond forming with a barrier of 29.8 kcal mol^{-1}. Alternatively, S14 can convert into the caged tetroxide intermediate S16 through asymmetric two step O_2-O_3 and O_5-O_6 bonds scission with the barriers of 19.1 and 3.1 kcal mol^{-1}, respectively. The result shows that the latter pathway is preferred over the former channel owing to its lower barrier. The overall spin multiplicity of S16 is singlet, in which the O_2 moiety maintains the triplet ground state (spin up) and is very loosely

bound. In order to preserve overall singlet multiplicity, the two $HOCH_2O$ radical pairs ($^3(HOCH_2O\cdots HOCH_2O)$) must have triplet multiplicity (spin down). S16 can be regarded as the ground state $^3O_2$ moving away from the two $HOCH_2O$ radical pairs that keep interacting. Due to the difficulty in performing the constrained optimization for the dissociation of S16, the $^3O_2$ moiety is considered as a leaving moiety away from two $HOCH_2O$ radical pairs, and merely the dissociation of $^3(HOCH_2O\cdots HOCH_2O)$ is taken into consideration in the present study. It has three types of pathways: (1) it yields $HOCH_2OH$ and excited-state ^3HCOOH through an alpha hydrogen transfer with a barrier of 14.0 kcal·mol^{-1} and 10.2 kcal·mol^{-1} exothermicity, followed by the excited ^3HCOOH to go back to the ground-state ^1HCOOH; (2) it generates two $HOCH_2O$ radicals via a barrierless process with the exoergicity of 16.9 kcal·mol^{-1}; (3) it produces dimer S17 via an intersystem crossing (ISC) step with the exoergicity of 32.1 kcal·mol^{-1}. Based on the calculated reaction barriers, the rate-limiting step is the cleavage of O_2-O_3 bond (R17) in the unimolecular decay processes of S14. This conclusion coincides with the previous result obtained from the dissociation of di-t-butyl tetroxide that the rate-controlling step is the rupturing of single O-O bond (Lee et al., 2016). Valiev et al. (2019) proposed that the ISC rate of ROOR dimer formed from various (RO···R'O) systems is extremely high (> 10^8 s^{-1}) and exhibits a strong stereoselectivity.

Figure 6 depicts a schematic PES for the self-reaction of $HOCH(CH_3)OO$ radical. As shown in Figure 6a, the self-reaction of $HOCH(CH_3)OO$ radical can produce either dimer S18 and $^1O_2$ via TS20 with a barrier of 44.4 kcal·mol^{-1}, or $HOCH(CH_3)OOH$ and $HOC(CH_3)OO$ through TS21 with a barrier of 54.3 kcal·mol^{-1}. But the barriers of R20 and R21 are considerably high, making them of less importance in the atmosphere. Alternatively, the self-reaction of $HOCH(CH_3)OO$ radical proceeds via an oxygen-to-oxygen coupling to form the tetroxide intermediate S19 with a barrier of 19.9 kcal·mol^{-1} (Figure 6b). The formed S19 proceeds through asymmetric two step O_2-O_3 and O_5-O_6 bonds scission to produce the caged tetroxide intermediate S21 of overall singlet multiplicity comprising two same-spin alkoxyl radicals (spin down) and triplet oxygen (spin up). These two processes overcome the

barriers of 21.4 and 1.3 kcal·mol^{-1}. Then, S21 decomposes into the propagation ($2HOCH(CH_3)O + {}^3O_2$) and termination products ($HOCH(CH_3)OH + {}^3CH_3OOH + {}^3O_2$ and dimer S22 + $^3O_2$) with the exoergicity of 12.5, 11.7 and 33.0 kcal·mol^{-1}. The rate-determining step is the rupturing of O_2-O_3 bond (R24) in the dissociation processes of S19.

As shown in Figure 7, the dominant pathway for the self-reaction of $HO(CH_3)_2COO$ radical begins with the formation of tetroxide intermediate S24 via an oxygen-to-oxygen coupling transition state TS28 with a barrier of 20.4 kcal·mol^{-1}; then it transforms into the caged tetroxide intermediate S26 of overall singlet spin multiplicity through asymmetric two-step O-O bond cleavage with the barriers of 22.0 and 3.4 kcal·mol^{-1}; finally, S26 can produce either two $HO(CH_3)_2CO$ radicals with the exoergicity of 10.3 kcal·mol^{-1}, or dimer S27 with the exoergicity of 31.5 kcal·mol^{-1}. Compared with the self-reactions of $HOCH_2OO$ and $HOCH(CH_3)OO$ radicals, the termination product of the self-reaction of $HOC(CH_3)_2OO$ radical is exclusively dimer S27 because of the absence of an alpha hydrogen atom in the $HOC(CH_3)_2OO$ radical. Compared with the barrier of the rate-determining route R17 in the self-reaction of $HOCH_2OO$ radical, the barrier of the rate-limiting step R29 is increased by about 3.0 kcal·mol^{-1} when two methyl substitutions are introduced at the C_1-position of $HOCH_2OO$ radical. The reason might be attributed to the cage escape of alkoxyl radicals. Therefore, tertiary RO_2 radicals have great opportunities to react with HO_2 radical or undergo autoxidation in pristine environments.

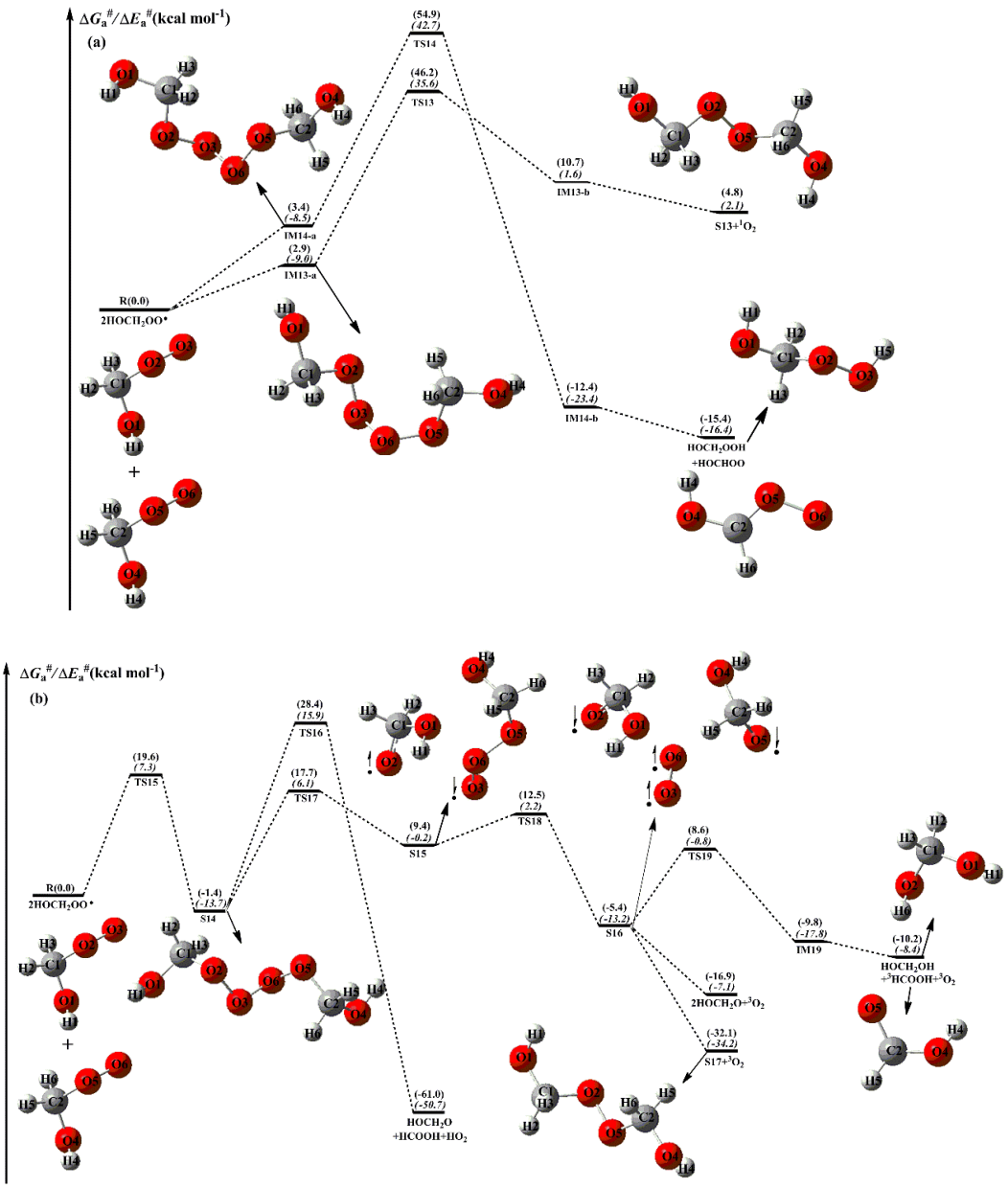

Figure 5. PES ($\Delta G_a^{\#}$ and $\Delta E_a^{\#}$, in italics) for the self-reaction of $HOCH_2OO$ radicals predicted at the M06-2X/ma-TZVP//M06-2X/6-311+G(2df,2p) level of theory

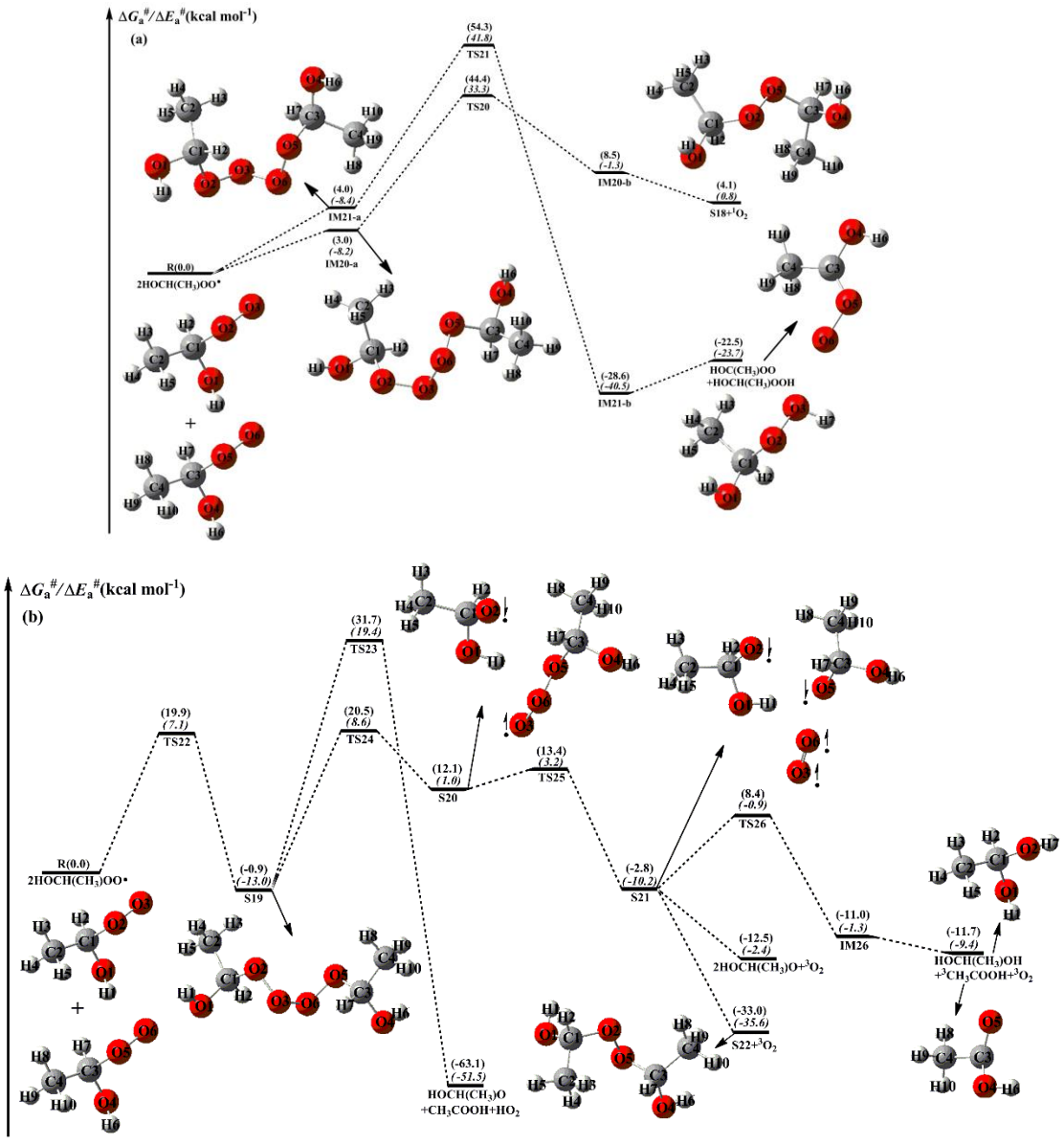

Figure 6. PES ($\Delta G_a^{\#}$ and $\Delta E_a^{\#}$, in italics) for the self-reaction of $HOCH(CH_3)OO$ radicals predicted at the M06-2X/ma-TZVP//M06-2X/6-311+G(2df,2p) level of theory

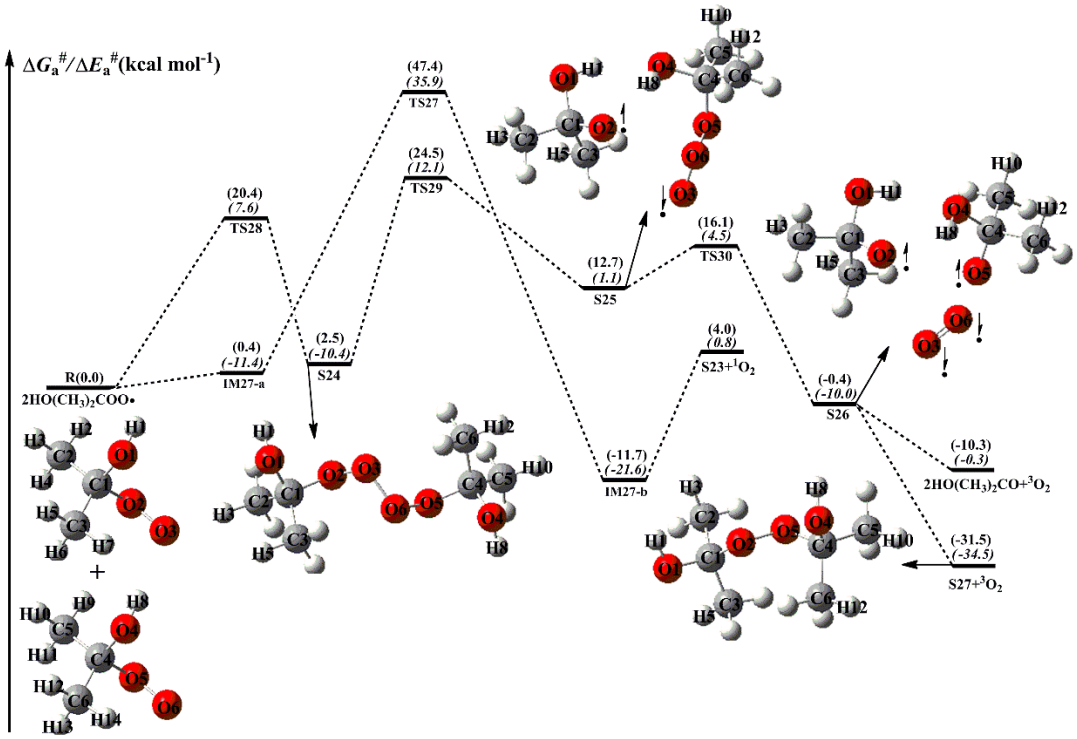

Figure 7. PES ($\Delta G_a^{\#}$ and $\Delta E_a^{\#}$, in italics) for the self-reaction of $HO(CH_3)_2COO$ radicals predicted at the M06-2X/ma-TZVP//M06-2X/6-311+G(2df,2p) level of theory

3.2.2 Reactions mechanism for the reaction of RO_2 radicals with HO_2 radical

When NO is present in low concentrations, the bimolecular reaction of RO_2 radicals with HO_2 radical is generally expected to be the dominant pathway. The primary sources of HO_2 radical include the photo-oxidation of oxygenated volatile organic compounds (OVOCs) and the ozonolysis reaction, as well as the secondary sources include the reactions of OH radical with CO, ozone and VOCs, the reaction of alkoxy radical RO with O_2, and the red-light-induced decomposition of α-hydroxy methylperoxy radical $OHCH_2OO$ (Kumar and Francisco, 2015; Stone et al., 2012; Hofzumahaus et al., 2009). The atmospheric concentration of HO_2 radical is 1.5-10 × 10^8 molecules cm^{-3} at the ground level in polluted urban environments (Stone et al., 2012). A schematic PES for the reactions of distinct RO_2 radicals with HO_2 radical is presented in Figure 8. As shown in Figure 8, all the reactions are strongly exothermic and spontaneous, indicating that they are thermodynamically feasible in the atmosphere. The reaction of $HOCH_2OO$ with HO_2 (R31) starts with the formation of a pre-reactive complex IM31-a in the entrance channel, which is more stable than the

separate reactants by 3.8 kcal mol^{-1}. Then, IM31-a converts into $HOCH_2OOH$ and O_2 via a hydrogen atom transfer from the HO_2 radical to the terminal oxygen atom of the $HOCH_2OO$ radical with a barrier of 2.0 kcal mol^{-1}. The mechanisms of $HOCH(CH_3)OO + HO_2$ (R32) and $HO(CH_3)_2COO + HO_2$ (R33) reactions are similar to that of the $HOCH_2OO + HO_2$ system. In order to avoid redundancy, a detailed discussion of the aforementioned mechanisms is not provided in the present study. Compared with the barrier of the $HOCH_2OO + HO_2$ reaction, the barrier height is lower by only 0.1 kcal mol^{-1} when one or two methyl substitutions occur at the C_1-position of $HOCH_2OO$ radical. This result suggests that the barrier height is not influenced by the number of methyl substitutions. The rate coefficients of the reactions of distinct RO_2 radicals with HO_2 radical are summarized in Table S5 and Figure S12. As shown in Table S5, the rate coefficients k_{R31} of the $HOCH_2OO + HO_2$ reaction vary from 3.1×10^{-11} (273 K) to 2.1×10^{-12} cm^3 molecule^{-1} s^{-1} (400 K), and they exhibit a negative temperature dependence. A similar conclusion is also obtained from the rate coefficients k_{R32} and k_{R33} that they decrease with the temperature increasing. Notably, the rate coefficient slightly increases when the number of methyl groups increases. At ambient temperature, k_{R31} is estimated to be 1.7×10^{-11} cm^3 molecule^{-1} s^{-1}, which is consistent with the value of $\sim 2 \times 10^{-11}$ cm^3 molecule^{-1} s^{-1} for the reaction of acyl peroxy radicals with HO_2 radical (Wennberg et al., 2018). The typical atmospheric concentrations of HO_2 radical are 5, 20 and 50 pptv in the urban, rural and forest environments, respectively (Bianchi et al., 2019), which translate into the pseudo-first-order rate constants $k'_{HO2} = k_{HO2}[HO_2]$ of 1.1×10^{-3}, 4.2×10^{-3} and 1.1×10^{-2} s^{-1}, respectively.

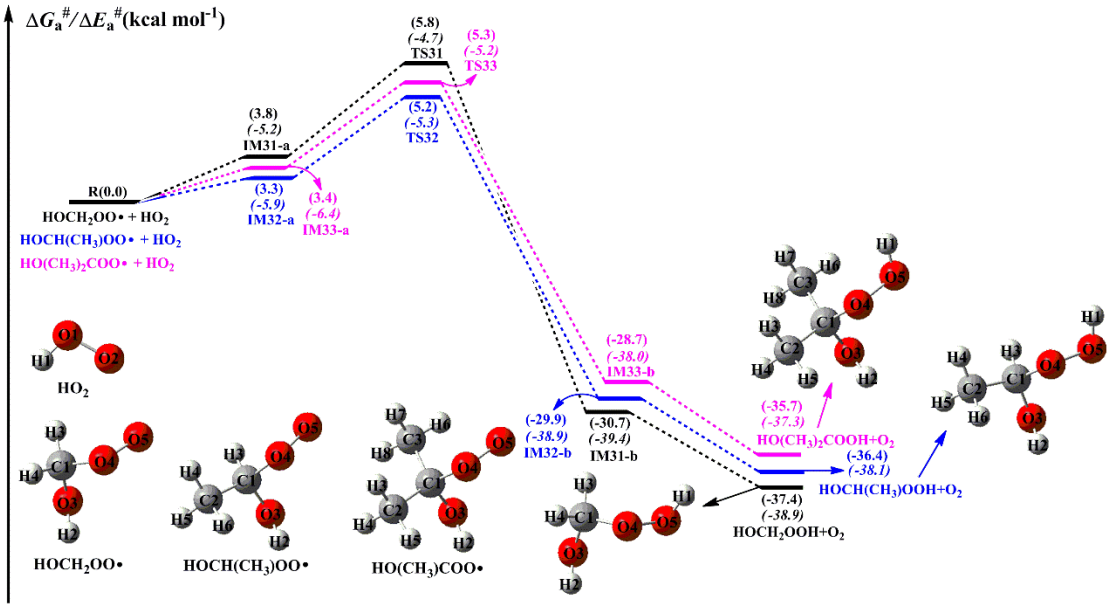

Figure 8. PES ($\Delta G_a^{\#}$ and $\Delta E_a^{\#}$, in italics) for the reactions of distinct RO_2 radicals with HO_2 radical predicted at the M06-2X/ma-TZVP//M06-2X/6-311+G(2df,2p) level of theory

3.2.3 Reactions mechanism for the isomerization of RO_2 radicals

The autoxidation of RO_2 radicals is known to play an important role in the (re)generation of HO_x radicals and the formation of HOMs (Xu et al., 2014; Bianchi et al., 2019; Rissanen et al., 2014; Ehn et al., 2017). The autoxidation mechanism includes an intramolecular H-shift from the $-CH_3$ or $-CH_2-$ groups to the -OO site, leading to the formation of a hydroperoxyalkyl radical QOOH, followed by O_2 addition to form a new peroxy radical ($HOOQO_2$), one after the other, resulting in the formation of HOMs (Rissanen et al., 2014; Berndt et al., 2015). For the H-shift reactions of RO_2 radicals, reactants, transition states and products have multiple conformers due to the effect of the degree of freedom for internal rotation. The calculated results show that the $HOCH_2OO$ radical has four energetically similar conformers ($HOCH_2OO$-a, $HOCH_2OO$-b, $HOCH_2OO$-c and $HOCH_2OO$-d). The relative free energy and Boltzmann population (w_i) of each individual conformer are listed in Table S6, which indicate that the Boltzmann populations of these four conformers are 46.39%, 46.31%, 2.99%, and 4.32%, respectively.

A schematic PES for the H-shift reaction of $HOCH_2OO$ radical is displayed in Figure 9. As can be seen in Figure 9, the lowest-energy conformer $HOCH_2OO$-a can proceed via a 1,3-H shift from the $-CH_2$ group to the terminal oxygen leading to the

formation of S28-a (HOCHOOH) with a barrier of 41.6 kcal mol^{-1}. $HOCH_2OO$-b can isomerize to S28-b1 and S28-b2 via the four-membered ring transition states TS34-b1 and TS34-b2 (1,3-H shifts) with the barriers of 41.6 and 45.0 kcal mol^{-1}, respectively. However, the 1,3-H shift reactions have comparatively high barriers, making them irrelevant in the atmosphere. Despite many attempts, the transition states of the H-shift reactions of $HOCH_2OO$-c and $HOCH_2OO$-d could not be located. The result suggests that the H-shift reactions of these two conformers are inhibited, which is consistent with the previous study that not all reactants will be in a conformation with a path across the barrier to reaction in the H-shift reactions of RO_2 radicals (Møller et al., 2016). Similar to the case of $HOCH_2OO$ radical, the isomerization of $HOCH(CH_3)OO$ radical proceeds via the 1,3- and 1,4-H shifts from the -CH or -CH_3 groups to the terminal oxygen resulting in the formation of hydroperoxyalkyl radicals (Figure S13). These 1,3- and 1,4-H shift reactions are accompanied by extremely high barriers (> 37.9 kcal mol^{-1}), indicating that they are of less importance in the atmosphere. A similar conclusion is also derived from the isomerization of $HO(CH_3)_2COO$ radical that 1,4-H shift reactions are unfavourable kinetically (Figure S14). The high barriers of the 1,3- and 1,4-H shifts can be interpreted as the result of the larger ring strain energy (RSE) in the cyclic transition state geometries. Consequently, the isomerization reactions of $HOCH_2OO$, $HOCH(CH_3)OO$ and $HO(CH_3)_2COO$ radicals are unlikely to proceed in the atmosphere. This conclusion is further supported by the previous studies that the intramolecular H-shift isomerizations are important only for RO_2 radicals with large carbon structures (Crounse et al., 2013; Jokinen et al., 2014; Rissanen et al., 2014).

The single-conformer rate coefficients ($k_{IRC\text{-}TST}$) and multi-conformer rate coefficients ($k_{MC\text{-}TST}$) of the isomerization of $HOCH_2OO$, $HOCH(CH_3)OO$ and $HOC(CH_3)_2OO$ radicals are calculated over the temperature range of 273-400 K as listed in Table S9-S11. As can be seen in Table S9, $k_{IRC\text{-}TST}$ of each conformer exhibits a marked positive temperature dependence over the temperature range studied. $k_{MC\text{-}TST}$ increases significantly with rising temperature, suggesting that a temperature increase promotes the isomerization of $HOCH_2OO$ radical. A similar conclusion is

also obtained for the isomerization of $HOCH(CH_3)OO$ and $HOC(CH_3)_2OO$ radicals (Table S10-S11). Notably, $k_{MC\text{-}TST}$ increases rapidly when the number of methyl groups increases. For example, the room temperature $k_{MC\text{-}TST}$ of $HOCH_2OO$ radical isomerization is calculated to be 4.4×10^{-16} s^{-1}, which is lower than those of the $HOCH(CH_3)OO$ (2.9×10^{-13} s^{-1}) and $HO(CH_3)_2COO$ (3.0×10^{-12} s^{-1}) radicals isomerization by 660 and 6820 times, respectively.

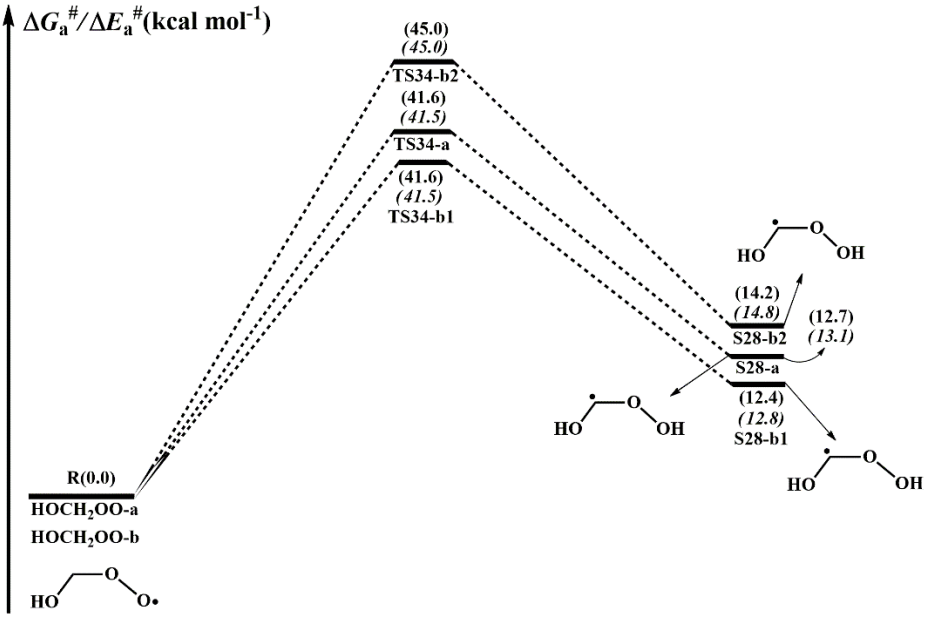

Figure 9. PES ($\Delta G_a^{\#}$ and $\Delta E_a^{\#}$, in italics) for the isomerization of $HOCH_2OO$ radical predicted at the M06-2X/ma-TZVP//M06-2X/6-311+G(2df,2p) level of theory

3.3 Subsequent reactions of H-abstraction products RO_2 radicals in urban environments

NO_x is present in high concentrations in urban environments, reaction with NO is the dominant chemical sink for RO_2 radicals (Atkinson and Arey, 2003; Orlando and Tyndall, 2012; Perring et al., 2013). The main pathways for this type of reaction lead to the formation of NO_2, RO radicals, organic nitrites, and organic nitrates at yields that are highly dependent on the nature of the R group (Orlando and Tyndall, 2012). The formation of NO_2 through subsequent photolysis ($\lambda < 420$ nm) produces ozone and NO, increasing the concentrations of near-surface ozone and propagating the NO_x chain (Orlando and Tyndall, 2012). The schematic PES for the reactions of distinct RO_2 radicals with NO are displayed in Figures 10-12. As shown in Figure 10, the bimolecular reaction of $HOCH_2OO$ radical with NO initially leads to the formation of

nitrite adduct S31 via the barrierless addition of NO to the terminal oxygen atom O_3 of $HOCH_2OO$ radical. The formed S31 exists two isomers: S31-*cis* refers to the O_2 and O_4 on the same side ($DO_2O_3N_1O_4$ = 2.3 °), whereas S31-*trans* refers to the O_2 and O_4 on the opposite side ($DO_2O_3N_1O_4$ = -179.8 °) with respect to the O_3-N_1 bond. The calculations show that S31-*cis* is more stable than S31-*trans* by 1.1 kcal·mol^{-1} in energy. Tautomerization between S31-*cis* and S31-*trans* proceeds through the rotation of O_3-N_1 bond with a barrier of 14.4 kcal·mol^{-1}, implying that they can be regarded as the separate atmospheric species. According to the Boltzmann-weighted distribution, the predicted proportions of S31-*cis* and S31-*trans* at room temperature are 86.5% and 13.5%, respectively. This result suggests that the dominant product of the reaction of $HOCH_2OO$ radical with NO is S31-*cis*, so it is selected as a model compound to insight into the mechanism of secondary reactions in the following sections.

S31-*cis* can either isomerize to organic nitrate S32 (R38) via a concerted process of O_2-O_3 bond breaking and O_2-N_1 bond forming with a barrier of 47.8 kcal·mol^{-1}, or decompose into $HOCH_2O$ radical and NO_2 (R39) via the cleavage of O_2-O_3 bond with a barrier of 11.3 kcal·mol^{-1}. The result shows that the latter pathway is more favourable than the former channel. A similar conclusion is also obtained from the reactions of NO with $HOCH(CH_3)OO$ and $HO(CH_3)_2COO$ radicals that the formation of organic nitrate is of minor importance in the atmosphere. This result is further supported by the prior studies that the direct formation of organic nitrate from peroxy nitrites is a minor channel for the reactions of isoprene-derived RO_2 radicals with NO (Piletic et al., 2017; Zhang et al., 2002). It should be noted that the transition state TS39 is not located using the M06-2X functional, but it is located at the MP2/6-311+G(2df,2p) level of theory and is verified using IRC calculations. The formed $HOCH_2O$ radical has two possible pathways: (1) it directly decomposes into CH_2O and OH radical (R40) via β-site C_1-O_1 bond scission with a barrier of 52.4 kcal·mol^{-1}; (2) it converts into HCOOH and HO_2 radical (R41) through H-abstraction by O_2 with a barrier of 26.4 kcal·mol^{-1}. This result reveals that R41 is the most feasible channel in the fragmentation of $HOCH_2O$ radical.

From Figure 11, it can be seen that the addition of NO to $HOCH(CH_3)OO$ radical

leading to the formation of S33-*cis* is barrierless. Then, it decomposes into $HOCH(CH_3)O$ radical and NO_2 (R44) via the cleavage of O_2-O_3 bond with a barrier of 11.5 kcal mol^{-1}. The resulting $HOCH(CH_3)O$ radical has three possible pathways. The first is the β-site C_1-C_2 bond scission leading to the formation of HCOOH + CH_3 (R45) with a barrier of 8.3 kcal mol^{-1}. The second is the β-site C_1-O_1 bond cleavage resulting in the formation of CH_3COH + OH (R46) with a barrier of 26.7 kcal mol^{-1}. The third is H-abstraction by O_2 leading to CH_3COOH + HO_2 (R47) with a barrier of 26.2 kcal mol^{-1}. On the basis of the calculated reaction barriers, the β-site C_1-C_2 bond scission is the dominant pathway in the fragmentation of $HOCH(CH_3)O$ radical. This conclusion is further supported by the previous experimental result that β-hydroxy intermediates primarily undergo decomposition rather than react with O_2 in the presence of NO (Aschmann et al., 2000). Equivalent to the $HOCH(CH_3)OO$ + NO reaction, the bimolecular reaction of $HO(CH_3)_2COO$ radical with NO has similar transformation pathways (Figure 12). The reaction of $HO(CH_3)_2COO$ with NO initially proceeds via a barrierless addition leading to S35-*cis* with a binding energy of 12.6 kcal mol^{-1}. Then, S35-*cis* fragments into $HO(CH_3)_2CO$ radical and NO_2 (R50) via the cleavage of O_2-O_3 bond with a barrier of 11.4 kcal mol^{-1}. The formed $HO(CH_3)_2CO$ radical can either dissociate into CH_3COOH + CH_3 (R51) via the scission of C_1-C_3 bond with a barrier of 8.2 kcal mol^{-1}, or decompose into CH_3COCH_3 + OH (R52) through the cleavage of C_1-O_1 bond with a barrier of 24.3 kcal mol^{-1}. This result also shows that the β-site C-C bond scission is the dominant pathway.

The typical atmospheric concentrations of NO are around 10 ppbv, 1 ppbv, and 20 pptv in the urban, rural, and forest environments, respectively (Bianchi et al., 2019). The rate coefficient of $HOCH_2OO$ radical reaction with NO is calculated to be 4.3×10^{-12} cm^3 $molecule^{-1}$ s^{-1} at room temperature, resulting in the pseudo-first-order rate constants $k'_{NO} = k_{NO}[NO]$ of 6.5×10^{-1}, 6.5×10^{-2}, and 1.3×10^{-3}, respectively, in the urban, rural, and forest environments. It is of interest to assess the relative importance for the H-shift reaction of $HOCH_2OO$ radical and bimolecular reactions with HO_2 radical and NO based on the calculated $k_{MC\text{-}TST}$, k'_{HO2} and k'_{NO}. It can be

found that the H-shift reaction is of less importance, and the HO_2 radical reaction is favorable in the forest environments, and the NO reaction is predominant in the urban and rural environments. A similar conclusion is also obtained from the cases of $HOCH(CH_3)OO$ and $HO(CH_3)_2CHOO$ radicals.

The rate coefficients of the dominant pathways of $HOCH_2O$, $HOCH(CH_3)O$ and $HO(CH_3)_2CHO$ radical fragmentations are summarized in Table S12. As can be seen in Table S12, k_{R41} increases slightly with the temperature increasing, and the discrepancy is about a factor of 12 at the two extremes of the studied temperature range. At the ground level with $[O_2]$ = ~ 5.0 × 10^{18} molecule cm^{-3}, the pseudo-first-order rate constant $k'_{O2} = k_{R41}[O_2]$ is estimated to be 38.0 s^{-1} at room temperature. k_{R45} varies significantly from 2.0 × 10^6 (273 K) to 3.1 × 10^8 (400 K) s^{-1}, and it exhibits a marked positive temperature dependence. A similar phenomenon is observed for k_{R51} that k_{R51} increases significantly with increasing temperature. k_{R51} is greater than k_{R45} by a factor of ~1.3, suggesting that the rate coefficient of β-site C-C bond scission increases slightly when the number of methyl groups increases.

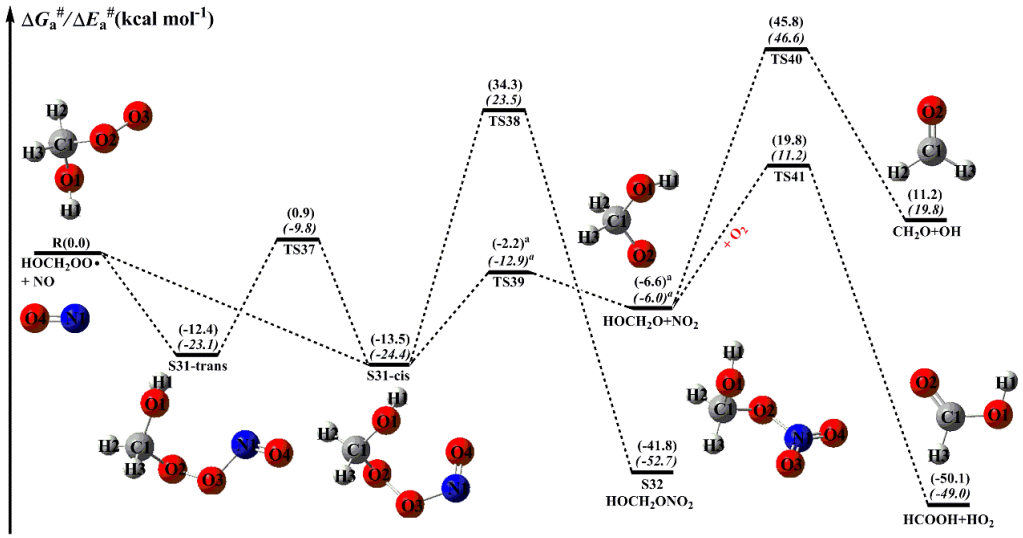

Figure 10. PES ($\Delta G_a^{\#}$ and $\Delta E_a^{\#}$, in italics) for the reaction of $HOCH_2OO$ radical with NO predicted at the M06-2X/ma-TZVP//M06-2X/6-311+G(2df,2p) level of theory (the superscript a is calculated at the MP2/ma-TZVP//MP2/6-311+G(2df,2p) level)

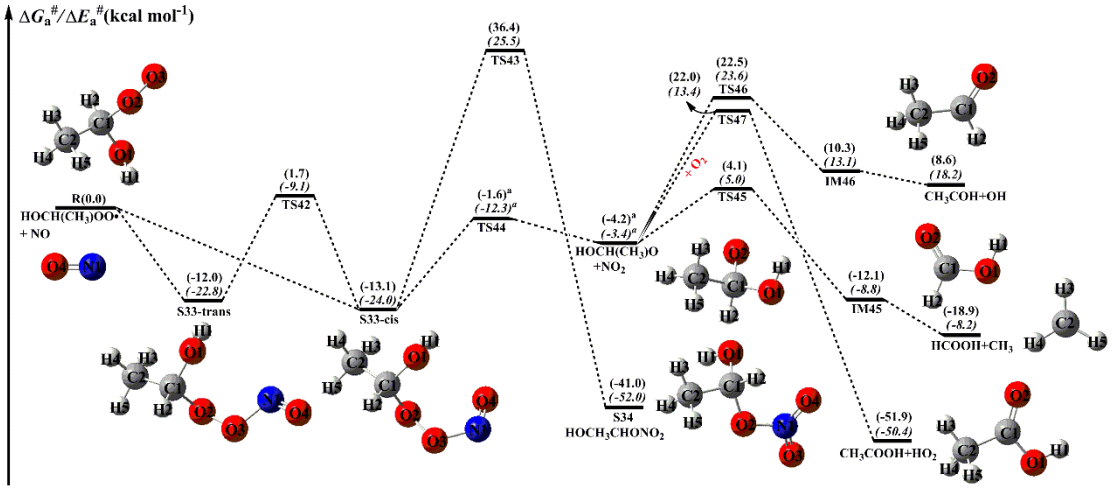

Figure 11. PES ($\Delta G_a^{\#}$ and $\Delta E_a^{\#}$, in italics) for the reaction of $HOCH(CH_3)OO$ radical with NO predicted at the M06-2X/ma-TZVP//M06-2X/6-311+G(2df,2p) level of theory (the superscript a is calculated at the MP2/ma-TZVP//MP2/6-311+G(2df,2p) level)

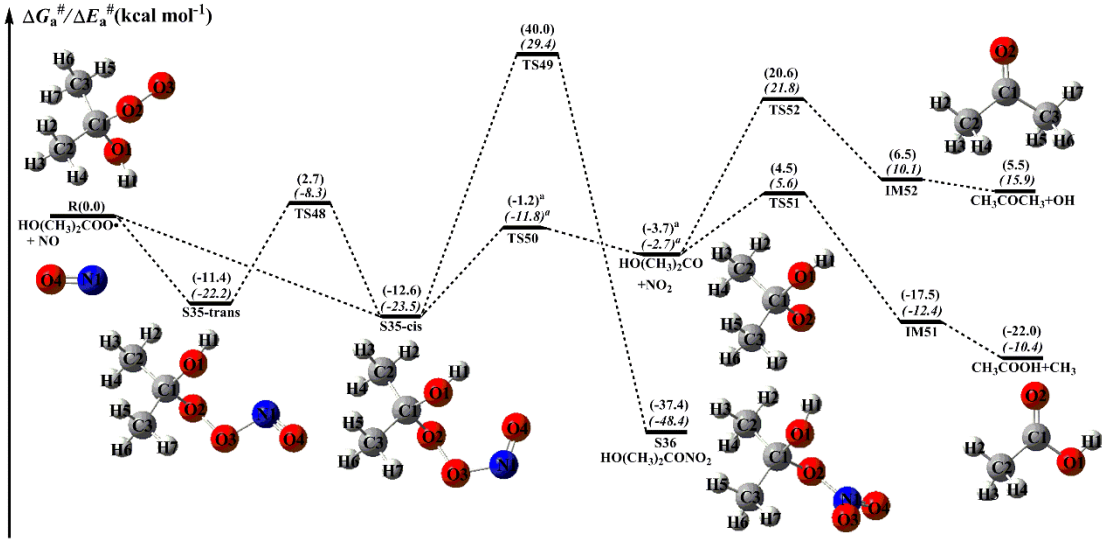

Figure 12. PES ($\Delta G_a^{\#}$ and $\Delta E_a^{\#}$, in italics) for the reaction of $HO(CH_3)_2COO$ radical with NO predicted at the M06-2X/ma-TZVP//M06-2X/6-311+G(2df,2p) level of theory (the superscript a is calculated at the MP2/ma-TZVP//MP2/6-311+G(2df,2p) level)

4. Conclusions

The detailed mechanisms and kinetic properties of OH-initiated oxidation of distinct HHPs and the subsequent transformation of resulting H-abstraction products are investigated using quantum chemical and kinetics modeling methods. The main conclusions are summarized as follows:

(a) The dominant pathway is H-abstraction from the -OOH group in the initiation reactions of OH radical with $HOCH_2OOH$ and $HOC(CH_3)_2OOH$. H-abstraction from the -CH group is competitive with that from the -OOH group in

692 the reaction of OH radical with $HOCH(CH_3)OOH$. The barrier of H-abstraction from
693 the -OOH group slightly increases when the number of methyl groups increases.
694 Compared with the rate coefficient of dominant pathway in the parent system, it is
695 almost identical when a methyl group substitution occurs at the C_1-position, whereas
696 it reduces by a factor of 2-5 when two methyl groups are introduced at the C_1-position.
697 The atmospheric lifetimes of $HOCH_2OOH$, $HOCH(CH_3)OOH$ and $HOC(CH_3)_2OOH$
698 reactivity toward OH radical are estimated to be 0.58-1.74 h, 0.60-1.79 h and
699 1.23-3.69 h, respectively, at room temperature under the typical OH radical
700 concentrations of 5-15 $\times 10^6$ molecules cm^{-3} during daylight.

701 (b) The self-reaction of RO_2 radical initially produces a tetroxide intermediate
702 via an oxygen-to-oxygen coupling, then it decomposes into propagation and
703 termination products through asymmetric two-step O-O bond scission. The
704 rate-limiting step is the first O-O bond cleavage, and the barrier increases when the
705 number of methyl groups increases. This finding contributes toward the understanding
706 of the self-reaction of complex RO_2 radicals.

707 (c) The bimolecular reactions of distinct RO_2 radicals with HO_2 radical lead to
708 the formation of hydroperoxide ROOH as the main product, and the barrier height is
709 not affected by the number of methyl substitutions. Compared with the rate coefficient
710 for the $HOCH_2OO + HO_2$ reaction, the rate coefficients increase by a factor of 2-5
711 when one or two methyl groups are introduced at the C1-position. Using a HO_2
712 radical concentration of ~50 pptv in the forest environments, the pseudo-first-order
713 rate constants k'_{HO2} of the reactions of distinct RO_2 radicals with HO_2 radical vary
714 from 1 to 5 $\times 10^{-2}$ s^{-1}.

715 (d) The isomerization reactions of $HOCH_2OO$, $HOCH(CH_3)OO$ and
716 $HO(CH_3)_2COO$ radicals are unlikely to proceed in the atmosphere because the
717 intramolecular H-shift steps have considerably high barriers and are strongly
718 endergonic. The result suggests that the isomerization of RO_2 radicals with small
719 carbon structures is of less importance in the atmosphere.

720 (e) The reaction with O_2 to form formic acid and HO_2 radical is the dominant
721 removal pathway for $HOCH_2O$ radical formed from the reaction of $HOCH_2OO$

radical with NO. The β-site C-C bond scission is the dominant pathway in the dissociation of $HOCH(CH_3)O$ and $HOC(CH_3)_2O$ radicals formed from the reactions of NO with $HOCH(CH_3)OO$ and $HOC(CH_3)_2OO$ radicals. The result suggests that methyl-substituted alkoxyl radicals primarily proceed via β-site C-C bond scission to produce aldehyde or carbonyl.

Data availability

The data are accessible by contacting the corresponding author (huangyu@ieecas.cn).

Supplement

The following information is provided in the Supplement: Y//X (Y = M06-2X, CCSD(T), X = 6-311+G(2df,2p), ma-TZVP) calculated energy barrier ($\Delta E_a^{\#}$, $\Delta G_a^{\#}$) for the OH + HHPs reactions; Rate coefficients of each elementary pathway involved in the initiation reactions of OH radical with $HOCH_2OOH$, $HOCH(CH_3)OOH$ and $HO(CH_3)_2COOH$; Rate coefficients of HO_2 radical reactions with $HOCH_2OO$, $HOCH(CH_3)OO$ and $HO(CH_3)_2COO$ radicals; The relative free energy and Boltzmann populations (w_i) of the conformer of $HOCH_2OO$, $HOCH(CH_3)OO$ and $HO(CH_3)_2COO$ radicals; The single-conformer rate coefficients ($k_{IRC\text{-}TST}$) and multi-conformer rate coefficients ($k_{MC\text{-}TST}$) of $HOCH_2OO$, $HOCH(CH_3)OO$ and $HO(CH_3)_2COO$ radicals; Rate coefficients of dominant pathways in the $HOCH_2OO\cdot$ + NO, $HOCH(CH_3)OO\cdot$ + NO and $HO(CH_3)_2CHOO\cdot$ + NO reactions; PESs ($\Delta E_a^{\#}$) for the OH-initiated reactions of $HOCH_2OOH$, $HOCH(CH_3)OOH$ and $HOC(CH_3)_2OOH$; Geometries of all the stationary points; Plots of the rate coefficients of each elementary pathway versus temperature; PESs ($\Delta G_a^{\#}$ and $\Delta E_a^{\#}$, in italics) for the isomerization of $HOCH(CH_3)OO$ and $HO(CH_3)_2COO$ radicals.

Author contribution

LC designed the study. LC and YH wrote the paper. LC performed theoretical calculation. YX, ZJ, and WW analyzed the data. All authors reviewed and commented on the paper.

Competing interests

The authors declare that they have no conflict of interest.

Acknowledgments

This work was supported by the National Natural Science Foundation of China (grant Nos. 42175134, 41805107, and 22002080). It was also partially supported as Key Projects of Chinese Academy of Sciences, China (grant No. ZDRW-ZS-2017-6), Strategic Priority Research Program of the Chinese Academy of Sciences, China (grant Nos. XDA23010300 and XDA23010000), Key Project of International Cooperation of the Chinese Academy of Sciences, China (grant No. GJHZ1543), Research Grants Council of Hong Kong, China (grant No. PolyU 152083/14E), CAS "Light of West China" Program (XAB2019B01) and the General Project of Shaanxi Province (2020JQ-432).

References

Allen, H. M., Crounse, J. D., Bates, K. H., Teng, A. P., Krawiec-Thayer, M. P., Rivera-Rios, J. C., Keutsch, F. N., Clair, J. M. S., Hanisco, T. F., Møller, K. H., Kjaergaard, H. G., and Wennberg, P. O.: Kinetics and product yields of the OH initiated oxidation of hydroxymethyl hydroperoxide, J. Phys. Chem. A, 122, 6292-6302, https://doi.org/10.1021/acs.jpca.8b04577, 2018.

Anglada, J. M., and Solé, A.: Impact of the water dimer on the atmospheric reactivity of carbonyl oxides, Phys. Chem. Chem. Phys., 18, 17698-17712, https://doi.org/10.1039/C6CP02531E, 2016.

Anglada, J. M., González, J., and Torrent-Sucarrat, M.: Effects of the substituents on the reactivity of carbonyl oxides. a theoretical study on the reaction of substituted carbonyl oxides with water, Phys. Chem. Chem. Phys., 13, 13034-13045, https://doi.org/10.1039/c1cp20872a, 2011.

Aschmann, S. M., Arey, J., and Atkinson, R.: Formation of β-hydroxycarbonyls from the OH

radical-initiated reactions of selected alkenes, Environ. Sci. Technol., 34, 1702-1706, https://doi.org/10.1021/es991125a, 2000.

Atkinson, R., and Arey, J.: Atmospheric degradation of volatile organic compounds, Chem. Rev., 103, 4605-4638, https://doi.org/10.1021/cr0206420, 2003.

Bach, R. D., Dmitrenko, O., and Estévez, C. M.: Chemical behavior of the biradicaloid (HO ··ONO) singlet states of peroxynitrous acid. the oxidation of hydrocarbons, sulfides, and selenides, J. Am. Chem. Soc., 127, 3140-3155, https://doi.org/10.1021/ja044245d, 2005.

Berndt, T., Richters, S., Kaethner, R., Voigtländer, J., Stratmann, F., Sipilä, M., Kulmala, M., and Herrmann, H.: Gas-phase ozonolysis of cycloalkenes: formation of highly oxidized RO_2 radicals and their reactions with NO, NO_2, SO_2, and Other RO_2 radicals, J. Phys. Chem. A, 119, 10336-10348, https://doi.org/10.1021/acs.jpca.5b07295, 2015.

Berndt, T., Scholz, W., Mentler, B., Fischer, L., Herrmann, H., Kulmala, M., and Hansel, A.: Accretion product formation from self- and cross-reactions of RO_2 radicals in the atmosphere, Angew. Chem. Int. Ed., 57, 3820-3824, https://doi.org/10.1002/anie.201710989, 2018.

Bianchi, F., Kurten, T., Riva, M., Mohr, C., Rissanen, M. P., Roldin, P., Berndt, T., Crounse, J. D., Wennberg, P. O., Mentel, T. F., Wildt, J., Junninen, H., Jokinen, T., Kulmala, M., Worsnop, D. R., Thornton, J. A., Donahue, N., Kjaergaard, H. G., and Ehn, M.: Highly oxygenated organic molecules (HOM) from gas-phase autoxidation involving peroxy radicals: a key contributor to atmospheric aerosol, Chem. Rev., 119, 3472-3509, https://doi.org/10.1021/acs.chemrev.8b00395, 2019.

Boys, S. F., and Bernardi, F.: The calculation of small molecular interactions by the differences of separate total energies. Some procedures with reduced errors, Mol. Phys., 19, 553-566, https://doi.org/10.1080/00268977000101561, 1970.

Chao, W., Hsieh, J. T., Chang, C. H., and Lin, J. J. M.: Direct kinetic measurement of the reaction of the simplest Criegee intermediate with water vapor, Science, 347, 751-754, https://doi.org/10.1126/science.1261549, 2015.

Chen, L., Huang, Y., Xue, Y., Cao, J., and Wang, W.: Competition between HO_2 and H_2O_2 reactions with CH_2OO/*anti*-CH_3CHOO in the oligomer formation: a theoretical perspective, J. Phys. Chem. A, 121, 6981-6991, https://doi.org/10.1021/acs.jpca.7b05951, 2017.

Chen, L., Huang, Y., Xue, Y., Jia, Z., and Wang, W.: Atmospheric oxidation of 1-butene initiated by OH radical: Implications for ozone and nitrous acid formations, Atmos. Environ., 244, 118010-118021, https://doi.org/10.1016/j.atmosenv.2020.118010, 2021.

Chen, L., Huang, Y., Xue, Y., Shen, Z., Cao, J., and Wang, W.: Mechanistic and kinetics investigations of oligomer formation from Criegee intermediate reactions with hydroxyalkyl hydroperoxides, Atmos. Chem. Phys., 19, 4075-4091, https://doi.org/10.5194/acp-19-4075-2019, 2019.

Chen, L., Wang, W., Wang, W., Liu, Y., Liu, F., Liu, N., and Wang, B.: Water-catalyzed decomposition of the simplest Criegee intermediate CH_2OO, Theor. Chem. Acc., 135, 131-143, https://doi.org/10.1007/s00214-016-1894-9, 2016b.

Chen, L., Wang, W., Zhou, L., Wang, W., Liu, F., Li, C., and Lü, J.: Role of water clusters in the reaction of the simplest Criegee intermediate CH_2OO with water vapour, Theor. Chem. Acc., 135, 252-263, https://doi.org/10.1007/s00214-016-1998-2, 2016a.

Chhantyal-Pun, R., Welz, O., Savee, J. D., Eskola, A. J., Lee, E. P. F., Blacker, L., Hill, H. R., Ashcroft, M., Khan, M. A. H., Lloyd-Jones, G. C., Evans, L., Rotavera, B., Huang, H.,

826 Osborn, D. L., Mok, D. K. W., Dyke, J. M., Shallcross, D. E., Percival, C. J., Orr-Ewing, A. J.,
827 and Taatjes, C. A.: Direct measurements of unimolecular and bimolecular reaction kinetics of
828 the Criegee intermediate $(CH_3)_2COO$, J. Phys. Chem. A, 121, 4-15,
829 https://doi.org/10.1021/acs.jpca.6b07810, 2017.
830 Crounse, J. D., Nielsen, L. B., Jørgensen, S., Kjaergaard, H. G., and Wennberg, P. O.:
831 Autoxidation of organic compounds in the atmosphere, J. Phys. Chem. Lett., 4, 3513-3520,
832 https://doi.org/10.1021/jz4019207, 2013.
833 Dillon, T. J., and Crowley, J. N.: Direct detection of OH formation in the reactions of HO_2 with
834 $CH_3C(O)O_2$ and other substituted peroxy radicals, Atmos. Chem. Phys., 8, 4877-4889,
835 https://doi.org/10.5194/acp-8-4877-2008, 2008.
836 Eckart, C.: The penetration of a potential barrier by electrons, Phys. Rev., 35, 1303-1309,
837 https://doi.org/10.1103/PhysRev.35.1303, 1930.
838 Ehn, M., Berndt, T., Wildt, J., and Mentel, T.: Highly oxygenated molecules from atmospheric
839 autoxidation of hydrocarbons: a prominent challenge for chemical kinetics studies, Int. J.
840 Chem. Kinet., 49, 821-831, https://doi.org/10.1002/kin.21130, 2017.
841 Ehn, M., Thornton, J. A., Kleist, E., Sipilä, M., Junninen, H., Pullinen, I., Springer, M., Rubach, F.,
842 Tillmann, R., Lee, B., Lopez-Hilfiker, F., Andres, S., Acir, I. H., Rissanen, M., Jokinen,T.,
843 Schobesberger, S., Kangasluoma, J., Kontkanen, J., Nieminen, T., Kurtén, T., Nielsen, L. B.,
844 Jørgensen, S., Kjaergaard, H. G., Canagaratna, M., Maso, M. D., Berndt, T., Petäjä, T.,
845 Wahner, A., Kerminen, V. M., Kulmala, M., Worsnop, D. R., Wildt, J., and Mentel T. F.: A
846 large source of low-volatility secondary organic aerosol, Nature, 506, 476-479,
847 https://doi.org/10.1038/nature13032, 2014.
848 Fernández-Ramos, A., Ellingson, B. A., Meana-Pañeda, R., Marques, J. M. C., and Truhlar, D. G.:
849 Symmetry numbers and chemical reaction rates, Theor. Chem. Acc., 118, 813-826,
850 https://doi.org/10.1007/s00214-007-0328-0, 2007.
851 Francisco, J. S., and Eisfeld, W.: Atmospheric oxidation mechanism of hydroxymethyl
852 hydroperoxide, J. Phys. Chem. A, 113, 7593-7600, https://doi.org/10.1021/jp901735z, 2009.
853 Frisch, M. J., Trucks, G. W., Schlegel, H. B., Scuseria, G. E., Robb, M. A., Cheeseman, J. R.,
854 Montgomery, J. A. Jr., Vreven, T., Kudin, K. N., Burant, J. C., Millam, J. M., Iyengar, S. S.,
855 Tomasi, J., Barone, V., Mennucci. B., Cossi, M., Scalmani, G., Rega, N., Petersson, G. A.,
856 Nakatsuji, H., Hada, M., Ehara, M., Toyota, K., Fukuda, R., Hasegawa, J., Ishida, M.,
857 Nakajima, T., Honda, Y., Kitao, O., Nakai, H., Klene, M., Li, X., Knox, J. E., Hratchian, H. P.,
858 Cross, J. B., Adamo, C., Jaramillo, J., Gomperts, R., Stratmann, R. E., Yazyev, O., Austin, A.
859 J., Cammi, R., Pomelli, C., Ochterski, J. W., Ayala, P. Y., Morokuma, K., Voth, G. A.,
860 Salvador, P., Dannenberg, J. J., Zakrzewski, V. G., Dapprich, S., Daniels, A. D., Strain, M. C.,
861 Farkas, O., Malick, D. K., Rabuck, A. D., Raghavachari, K., Foresman, J. B., Ortiz, J. V., Cui,
862 Q., Baboul, A. G., Clifford, S., Cioslowski, J., Stefanov, B. B., Liu, G., Liashenko, A.,
863 Piskorz, P., Komaromi, I., Martin, R. L., Fox, D. J., Keith, T., Al-Laham, M. A., Peng, C. Y.,
864 Nanayakkara, A., Challacombe, M., Gill, P. M. W., Johnson, B., Chen, W., Wong, M. W.,
865 Gonzalez, C., and Pople, J. A.: Gaussian 09, Revision D.01; Gaussian, Inc.: Wallingford, CT,
866 2009.
867 Fukui, K.: The path of chemical reactions - the IRC approach, Acc. Chem. Res., 14, 363-368,
868 https://doi.org/10.1021/ar00072a001, 1981.
869 Gilbert, R. G., and Smith, S. C.: Theory of unimolecular and recombination reactions; Blackwell

Scientific: Carlton, Australia, 1990.
Gligorovski, S., Strekowski, R., Barbati, S., and Vione, D.: Environmental implications of hydroxyl radicals (OH), Chem. Rev., 115, 13051-13092, https://doi.org/10.1021/cr500310b, 2015.
Glowacki, D. R., Liang, C. H., Morley, C., Pilling, M. J., and Robertson, S. H.: MESMER: an open-source master equation solver for multi-energy well reactions, J. Phys. Chem. A, 116, 9545-9560, https://doi.org/10.1021/jp3051033, 2012.
Gong, Y., and Chen, Z.: Quantification of the role of stabilized Criegee intermediates in the formation of aerosols in limonene ozonolysis, Atmos. Chem. Phys., 21, 813-829, https://doi.org/10.5194/acp-21-813-2021, 2021.
Hofzumahaus, A., Rohrer, F., Lu, K., Bohn, B., Brauers, T., Chang, C. C., Fuchs, H., Holland, F., Kita, K., Kondo, Y., Li, X., Lou, S., Shao, M., Zeng, L., Wahner, A., and Zhang, Y.: Amplified trace gas removal in the troposphere, Science, 324, 1702-1704, https://doi.org/10.1126/science.1164566, 2009.
Holbrook, K. A., Pilling, M. J., Robertson, S. H., and Robinson, P. J.: Unimolecular reactions, 2nd ed.; Wiley: New York, 1996.
Huang, H. L., Chao, W., and Lin, J. J. M.: Kinetics of a Criegee intermediate that would survive high humidity and may oxidize atmospheric SO_2, Proc. Natl. Acad. Sci. U.S.A., 112, 10857-10862, https://doi.org/10.1073/pnas.1513149112, 2015.
Iyer, S., Reiman, H., Møller, K. H., Rissanen, M. P., Kjaergaard, H. G., and Kurtén, T.: Computational investigation of $RO_2 + HO_2$ and $RO_2 + RO_2$ reactions of monoterpene derived first-generation peroxy radicals leading to radical recycling, J. Phys. Chem. A, 122, 9542-9552, https://doi.org/10.1021/acs.jpca.8b09241, 2018.
Iyer, S., Rissanen, M. P., Valiev, R., Barua, S., Krechmer, J. E., Thornton, J., Ehn, M., and Kurtén, T.: Molecular mechanism for rapid autoxidation in α-pinene ozonolysis, Nat. Commun., https://doi.org/10.1038/s41467-021-21172-w, 12, 878-883, 2021.
Jara-Toro, R. A., Hernández, F. J., Garavagno, M. A., Taccone, R. A., and Pino, G. A.: Water catalysis of the reaction between hydroxyl radicals and linear saturated alcohols (ethanol and n-propanol) at 294 K, Phys. Chem. Chem. Phys., 20, 27885-27896, https://doi.org/10.1039/C8CP05411H, 2018.
Jara-Toro, R. A., Hernández, F. J., Taccone, R. A., Lane, S. I., and Pino, G. A.: Water catalysis of the reaction between methanol and OH at 294 K and the atmospheric implications, Angew. Chem., Int. Ed., 56, 2166-2170, https://doi.org/10.1002/anie.201612151, 2017.
Jokinen, T., Sipilä, M., Richters, S., Kerminen, V. M., Paasonen, P., Stratmann, F., Worsnop, D., Kulmala, M., Ehn, M., Herrmann, H., and Berndt, T.: Rapid autoxidation forms highly oxidized RO_2 radicals in the atmosphere, Angew. Chem. Int. Ed., 53, 14596-14600, https://doi.org/10.1002/anie.201408566, 2014.
Khan, M. A. H., Percival, C. J., Caravan, R. L., Taatjes, C. A., and Shallcross, D. E.: Criegee intermediates and their impacts on the troposphere, Environ. Sci.: Processes Impacts, 20, 437-453, https://doi.org/10.1039/C7EM00585G, 2018.
Kumar, M., and Francisco, J. S.: Red-light initiated decomposition of α-hydroxy methylperoxy radical in the presence of organic and inorganic acids: implications for the HO_x formation in the lower stratosphere, J. Phys. Chem. A, 120, 2677-2683, https://doi.org/10.1021/acs.jpca.6b01515, 2016.

Kumar, M., and Francisco, J. S.: Red-light-induced decomposition of an organic peroxy radical: a new source of the HO_2 radical, Angew. Chem. Int. Ed., 54, 15711-15714, https://doi.org/10.1002/anie.201509311, 2015.

Kumar, M., Busch, D. H., Subramaniam, Bala., and Thompson, W. H.: Role of tunable acid catalysis in decomposition of α-hydroxyalkyl hydroperoxides and mechanistic implications for tropospheric chemistry, J. Phys. Chem. A, 118, 9701-9711, https://doi.org/10.1021/jp505100x, 2014.

Lee, R., Gryn'ova, G., Ingold, K. U., and Coote, M. L.: Why are sec-alkylperoxyl bimolecular self-reactions orders of magnitude faster than the analogous reactions of tert-alkylperoxyls? The unanticipated role of CH hydrogen bond donation, Phys. Chem. Chem. Phys., 18, 23673-23679, https://doi.org/10.1039/C6CP04670C, 2016.

Lester, M. I., and Klippenstein, S. J.: Unimolecular decay of Criegee intermediates to OH radical products: prompt and thermal decay processes, Acc. Chem. Res., 51, 978-985, https://doi.org/10.1021/acs.accounts.8b00077, 2018.

Liu, L., Bei, N., Wu, J., Liu, S., Zhou, J., Li, X., Yang, Q., Feng, T., Cao, J., Tie, X., and Li, G.: Effects of stabilized Criegee intermediates (sCIs) on sulfate formation: a sensitivity analysis during summertime in Beijing-Tianjin-Hebei (BTH), China. Atmos. Chem. Phys., 19, 13341-13354, https://doi.org/10.5194/acp-19-13341-2019, 2019.

Long, B., Bao, J. L., and Truhlar, D. G.: Reaction of SO_2 with OH in the atmosphere, Phys. Chem. Chem. Phys., 19, 8091-8100, https://doi.org/10.1039/C7CP00497D, 2017.

Lu, T.: Molclus program, Version 1.9.3, http://www.keinsci.com/research/molclus.html (accessed Feb. 10, 2020).

Ma, F., Guo, X., Xia, D., Xie, H. B., Wang, Y., Elm, J., Chen, J., and Niu, J.: Atmospheric chemistry of allylic radicals from isoprene: a successive cyclization-driven autoxidation mechanism, Environ. Sci. Technol., 55, 4399-4409, https://doi.org/10.1021/acs.est.0c07925, 2021.

Møller, K. H., Berndt, T., and Kjaergaard, H. G.: Atmospheric autoxidation of amines, Environ. Sci. Technol., 54, 11087-11099, https://doi.org/10.1021/acs.est.0c03937, 2020.

Møller, K. H., Otkjær, R. V., Hyttinen, N., Kurtén, T., and Kjaergaard, H. G.: Cost-effective implementation of multiconformer transition state theory for peroxy radical hydrogen shift reactions, J. Phys. Chem. A, 120, 10072-10087, https://doi.org/10.1021/acs.jpca.6b09370, 2016.

Nozière, B., and Vereecken, L.: Direct observation of aliphatic peroxy radical autoxidation and water effects: an experimental and theoretical study, Angew. Chem. Int. Ed., 58, 13976-13982, https://doi.org/10.1002/anie.201907981, 2019.

Orlando, J. J., and Tyndall, G. S.: Laboratory studies of organic peroxy radical chemistry: an overview with emphasis on recent issues of atmospheric significance, Chem. Soc. Rev., 41, 6294-6317, https://doi.org/10.1039/c2cs35166h, 2012.

Perring, A. E., Pusede, S. E., and Cohen, R. C.: An observational perspective on the atmospheric impacts of alkyl and multifunctional nitrates on ozone and secondary organic aerosol, Chem. Rev., 113, 5848-5870, https://doi.org/10.1021/cr300520x, 2013.

Piletic, I. R., Edney, E. O., and Bartolotti, L. J.: Barrierless reactions with loose transition states govern the yields and lifetimes of organic nitrates derived from isoprene, J. Phys. Chem. A, 121, 8306-8321, https://doi.org/10.1021/acs.jpca.7b08229, 2017.

Qiu, J. T., Ishizuka, S., Tonokura, K., Colussi, A. J., and Enami, S.: Water dramatically accelerates the decomposition of α-hydroxyalkyl-hydroperoxides in aerosol particles, J. Phys. Chem. Lett., 10, 5748-5755, https://doi.org/10.1021/acs.jpclett.9b01953, 2019.

Rissanen, M. P., Kurtén, T., Sipilä, M., Thornton, J. A., Kangasluoma, J., Sarnela, N., Junninen, H., Jørgensen, S., Schallhart, S., Kajos, M. K., Taipale, R., Springer, M., Mentel, T. F., Ruuskanen, T., Petäjä, T., Worsnop, D. R., Kjaergaard, H. G., and Ehn, M.: The formation of highly oxidized multifunctional products in the ozonolysis of cyclohexene, J. Am. Chem. Soc., 136, 15596-15606, https://doi.org/10.1021/ja507146s, 2014.

Russell, G. A.: Deuterium-isotope effects in the autoxidation of aralkyl hydrocarbons. Mechanism of the interaction of peroxy radicals, J. Am. Chem. Soc., 79, 3871-3877, https://doi.org/10.1021/ja01571a068, 1957.

Ryzhkov, A. B., and Ariya, P. A.: A theoretical study of the reactions of carbonyl oxide with water in atmosphere: the role of water dimer, Chem. Phys. Lett., 367, 423-429, https://doi.org/10.1016/S0009-2614(02)01685-8, 2003.

Smith, M. C., Chang, C. H., Chao, W., Lin, L. C., Takahashi, K., Boering, K. A., and Lin, J. J. M.: Strong negative temperature dependence of the simplest Criegee intermediate CH_2OO reaction with water dimer, J. Phys. Chem. Lett., 6, 2708-2713, https://doi.org/10.1021/acs.jpclett.5b01109, 2015.

Stone, D., Whalley, L. K., and Heard, D. E.: Tropospheric OH and HO_2 radicals: field measurements and model comparisons, Chem. Soc. Rev., 41, 6348-6404, https://doi.org/10.1039/c2cs35140d, 2012.

Taatjes, C. A., Welz, O., Eskola, A. J., Savee, J. D., Scheer, A. M., Shallcross, D. E., Rotavera, B., Lee, E. P. F., Dyke, J. M., Mok, D. K. W., Osborn, D. L., and Percival, C. J.: Direct measurements of conformer-dependent reactivity of the Criegee intermediate CH_3CHOO, Science, 340, 177-180, https://doi.org/10.1126/science.1234689, 2013.

Taatjes, C. A.: Criegee intermediates: what direct production and detection can teach us about reactions of carbonyl oxides, Annu. Rev. Phys. Chem., 68, 183-207, https://doi.org/10.1146/annurev-physchem-052516-050739, 2017.

Valiev, R. R., Hasan, G., Salo, V. T., Kubečka, J., and Kurten, T.: Intersystem crossings drive atmospheric gas-phase dimer formation, J. Phys. Chem. A, 123, 6596-6604, https://doi.org/10.1021/acs.jpca.9b02559, 2019.

Wang, S., Riva, M., Yan, C., Ehn, M., and Wang, L.: Primary formation of highly oxidized multifunctional products in the OH-initiated oxidation of isoprene: a combined theoretical and experimental study, Environ. Sci. Technol., 52, 12255-12264, https://doi.org/10.1021/acs.est.8b02783, 2018.

Wang, S., Wu, R., Berndt, T., Ehn, M., and Wang, L.: Formation of highly oxidized radicals and multifunctional products from the atmospheric oxidation of alkylbenzenes, Environ. Sci. Technol., 51, 8442-8449, https://doi.org/10.1021/acs.est.7b02374, 2017.

Wennberg, P. O., Bates, K. H., Crounse, J. D., Dodson, L. G., McVay, R. C., Mertens, L. A., Nguyen, T. B., Praske, E., Schwantes, R. H., Smarte, M. D., Clair, J. M. S., Teng, A. P., Zhang, X., and Seinfeld, J. H.: Gas-phase reactions of isoprene and its major oxidation products, Chem. Rev., 118, 3337-3390, https://doi.org/10.1021/acs.chemrev.7b00439, 2018.

Winiberg, F. A. F., Dillon, T. J., Orr, S. C., Groß, C. B. M., Bejan, I., Brumby, C. A., Evans, M. J., Smith, S. C., Heard, D. E., and Seakins, P. W.: Direct measurements of OH and other product

yields from the HO_2 + $CH_3C(O)O_2$ reaction, Atmos. Chem. Phys., 16, 4023-4042, https://doi.org/10.5194/acp-16-4023-2016, 2016.

Xu, L., Kollman, M. S., Song, C., Shilling, J. E., and Ng, N. L.: Effects of NO_x on the volatility of secondary organic aerosol from isoprene photooxidation, Environ. Sci. Technol., 48, 2253-2262, https://doi.org/10.1021/es404842g, 2014.

Xu, L., Møller, K. H., Crounse, J. D., Kjaergaard, H. G., and Wennberg, P. O.: New insights into the radical chemistry and product distribution in the OH-initiated oxidation of benzene, Environ. Sci. Technol., 54, 13467-13477, https://doi.org/10.1021/acs.est.0c04780, 2020.

Zhang, D., Zhang, R., Park, J., and North, S. W.: Hydroxy peroxy nitrites and nitrates from OH initiated reactions of isoprene, J. Am. Chem. Soc., 124, 9600-9605, https://doi.org/10.1021/ja0255195, 2002.

Zhang, P., Wang, W., Zhang, T., Chen, L., Du, Y., Li, C., and Lv, J.: Theoretical study on the mechanism and kinetics for the self-reaction of $C_2H_5O_2$ radicals, J. Phys. Chem. A, 116, 4610-4620, https://doi.org/10.1021/jp301308u, 2012.

Zhao, Y., and Truhlar, D. G.: A new local density functional for main-group thermochemistry, transition metal bonding, thermochemical kinetics, and noncovalent interactions, J. Chem. Phys., 125, 194101-194119, https://doi.org/10.1063/1.2370993, 2006.

Zhao, Y., and Truhlar, D. G.: The M06 suite of density functionals for main group thermochemistry, thermochemical kinetics, noncovalent interactions, excited states, and transition elements: two new functionals and systematic testing of four M06-class functionals and 12 other functionals, Theor. Chem. Acc., 120, 215-241, https://doi.org/10.1007/s00214-007-0310-x, 2008.

Zheng, J., and Truhlar, D. G.: Direct dynamics study of hydrogen-transfer isomerization of 1-pentyl and 1-hexyl radicals, J. Phys. Chem. A, 113, 11919-11925, https://doi.org/10.1021/jp903345x, 2009.

Zheng, J., Xu, X., and Truhlar, D. G.: Minimally augmented Karlsruhe basis sets, Theor. Chem. Acc., 128, 295-305, https://doi.org/10.1007/s00214-010-0846-z, 2011.

Zhong, J., Kumar, M., Francisco, J. S., and Zeng, X. C.: Insight into chemistry on cloud/aerosol water surfaces, Acc. Chem. Res., 51, 1229-1237, https://doi.org/10.1021/acs.accounts.8b00051, 2018.

Zhou, X., Liu, Y., Dong, W., and Yang, X.: Unimolecular reaction rate measurement of *syn*-CH_3CHOO, J. Phys. Chem. Lett., 10, 4817-4821, https://doi.org/10.1021/acs.jpclett.9b01740, 2019.

Zhu, C., Kumar, M., Zhong, J., Li, L., Francisco, J. S., and Zeng, X. C.: New mechanistic pathways for Criegee-water chemistry at the air/water interface, J. Am. Chem. Soc., 138, 11164-11169, https://doi.org/10.1021/jacs.6b04338, 2016.